

Ion Cyclotron Waves in Space Plasmas

L. Gomberoff

*Departamento de Física, Facultad de Ciencias,
Universidad de Chile, Casilla 653, Santiago, Chile*

Received November 14, 1995

We study the linear and nonlinear properties of electromagnetic ion-cyclotron waves in the magnetosphere and the solar wind. In particular, we study parametric decays of large amplitude electromagnetic ion-cyclotron waves (EICW) due to a minor O^+ and He^+ ion components in the magnetosphere. It is shown that the presence of O^+ and He^+ ions lead to a number of new wave couplings which in turn lead to new instabilities. Some couplings involve sound waves carried mainly by the O^+ (He^+) ions, and a sideband electromagnetic ion-cyclotron wave which has a resonance at the O^+ (He^+) ion gyrofrequency. These are decay instabilities which can lead to O^+ and He^+ heating through Landau damping and/or resonance absorption. It is also shown that the decays to sound waves associated to the minority heavy ion species have growth rates comparable, or even larger, than the decays to the acoustic branch corresponding to the majority proton species. In a recent paper Hollweg et al. [1993] studied the parametric decay of Alfvén waves in high speed solar wind streams. Following this analysis we consider the nonlinear decay of left hand polarized ion-cyclotron waves. It is shown that in a solar wind type plasma composed of electrons, protons, and alpha particles drifting relative to the protons, both branches of the dispersion relation of the circularly polarized waves can be excited by observed thermal anisotropies [Gomberoff and Elgueta, 1991]. Guided by this analysis, the parametric decay of each branch of the dispersion relation is discussed. It is shown that the presence of drifting alpha particles introduces new wave couplings in the system which lead to new instabilities. Some of these instabilities involve sound waves supported essentially by the alpha particles which, due to Landau damping, can be very efficient in the energization of alpha particles. Other instabilities involve ordinary sound waves which can lead to proton heating. A modulational instability which involves two electromagnetic daughters is also found. We have also found that a strong pump can force decays of modes that do not satisfy the resonance conditions when the pump intensity is vanishingly small. Finally, it is shown that both branches of the dispersion relation - particularly the branch close to the Doppler shifted alpha particle resonance - are highly unstable even for small intensities of the pump wave.

I. Introduction

In the present paper we shall review recent work on linear and nonlinear stability of electromagnetic ion cyclotron waves (EICW) in the magnetosphere and in the solar wind. Since space plasmas are multicomponent plasmas, this is a study of EICW in multicomponent plasmas.

EICW are often observed in various regions of the magnetosphere with L values ranging from 3 to 15 [Erlandson et al., 1990; Anderson et al., 1992 a,b]. These waves have been thoroughly studied over the years and it is by now well known that the presence

of minor heavy ions plays an important role on the dispersive properties of the plasma [Cuperman et al., 1975; Gendrin and Roux, 1980; Young et al., 1981; Fraser, 1982; Gomberoff and Cuperman, 1982; Gendrin 1983a,b; Gomberoff and Elgueta, 1991; Gomberoff, 1992].

From observations made on board the GEOS 1 and 2, and ATS 6 satellites, it is known that when large amplitude EICW are detected, minor O^+ and He^+ are heated up to suprathermal energies of about 100 eV [Young et al., 1981; Mauk et al., 1981; Roux et al., 1982; Fraser, 1982; Mauk, 1983].

This phenomenon, has been studied by a number of

authors within the context of linear theory, and also using simulation techniques [Mauk, 1982, 1983; Berchem et al., 1983; Berchem and Gendrin, 1985; Tanaka, 1985; Omura et al., 1985]. From the linear theory of EICW it follows that maximum growth rates occur at frequencies far from the heavy ion gyrofrequency and, therefore, these waves cannot heat up the bulk of the heavy ions [Gendrin et al., 1984; Berchem and Gendrin, 1985; Omura et al., 1985; Gomberoff and Vega, 1987]. Therefore, although heating can occur within the linear theory, it seems that linear theory alone is not sufficient to account for the observations. However, observationally it is clear that energization occurs when waves generated in one region propagate to another region along gradients. This condition is probably required even when taking into account nonlinear decays.

The nonlinear stability of electromagnetic ion cyclotron waves (EICW) has been extensively studied over the years, particularly, the stability of whistlers and Alfvén waves [Galeev and Oraievskii, 1963; Lutmirski and Sudan, 1966; Sagdeev and Galeev, 1969; Hasegawa, 1972; Lashmore-Davies, 1973; Goldstein, 1978; Cohen and Dewar, 1974; Barnes and Hollweg, 1974].

Most of these studies have considered plasmas composed of electrons and protons using either the one-fluid or the two-fluid model [Lashmore-Davies, 1976; Derby, 1978; Sakai and Sonnerup, 1983; Longtin and Sonnerup, 1986; Hoshino and Goldstein, 1989; Viñas and Goldstein, 1992 a,b; Umeki and Terazawa, 1992]. A kinetic approach has been developed by Lee and Kaw [1972] and Kaw [1976]. Inhester [1990], using a drift-kinetic treatment, has shown that thermal effects reduce the maximum growth rates obtained in a fluid theory emphasizing, thus, the need for a full kinetic treatment of the problem.

In a recent paper [Gomberoff et al., 1995a], the parametric decays of EICW in a magnetospheric-like plasma, composed of protons and He^+ ions were investigated. It was shown that although both species can be heated up by parametric instabilities, parametric decays involving sound waves carried mainly by He^+ show unstable wavenumber gaps more sensitive to the growth of the pump wave intensity, suggesting a preferential heating of the He^+ ions.

We shall consider a magnetosphere-like plasma com-

posed of three ion-species. The plasma composition is the following: a minor hot proton component of about 10% of the total proton number, thermal protons, thermal He^+ ions and a minor thermal O^+ ion-component with typical ratios of 100: 10: 1, respectively. Note that in other magnetospheric scenarios, the O^+ ion concentration can take values as large as 10%, which can also be studied with the present model. There may also be energetic heavy ions coming from the ring current [see e. g., Cornwall and Shultz, 1979] but, as we shall see, they do not play a significant role on the parametric decays of EICW [Gomberoff et al., 1994b].

We shall see that decay instabilities involving sound waves carried mainly by the heavy ion-species, have growth/damping rates comparable or even larger than those associated to instabilities involving the sound wave of the proton majority ions, indicating that they are substantially heated by nonlinear decays of EICW.

Next, we study EICW in high speed solar wind streams where alpha particles are drifting relative to the main proton component [see Marsch, 1991, and references therein]. It has been recently shown that a relative drift between two ion species modifies the dispersion relation of circularly polarized EICW in two important ways [Gomberoff and Elgueta, 1991]. First, the stop band which exists around the heavy species gyrofrequency when there is no drift [see, e.g., Gomberoff and Cuperman, 1982; Isenberg, 1984] disappears in the presence of drifts. Second, the branch which, in the absence of drifts, has a resonance at the proton gyrofrequency - to be called the alpha branch because it is very close to the Doppler shifted frequency of the drifting species - extends now beyond the proton gyrofrequency.

Another property of high speed solar wind streams, is the fact that alpha particles are hotter than protons. It seems that their thermal velocities are equal, namely, $T_\alpha = 4T_p$. Moreover, at distances of 0.3 AU, the alpha particle temperature is higher than the temperature in the solar corona, indicating that the alpha particles - and also other heavy ions - are heated up in their transit from the sun to 0.3 AU [see Marsch, 1991].

Recently, Hollweg et al. [1993], using the new dispersion relation of the circularly polarized EICW, showed that the alpha-proton drift velocity introduces

wave couplings which lead to several new parametric instabilities. These couplings can provide a way of transferring energy from the pump wave to the protons and to the alpha particles. This can occur through resonant cyclotron interaction between the daughter waves and the ions and/or by Landau damping of the sound waves, provided that Landau damping or resonant absorption do not suppress the instability altogether.

Here we review a recent paper [Gomberoff et al., 1994], which extends the work of Hollweg et al. [1993], by studying the nonlinear stability of the alpha particle branch of the dispersion relation. This branch of the dispersion relation can also be excited in high speed solar wind streams [see Gomberoff and Elgueta, 1991]. Moreover, since the alpha particle branch is very close to the Doppler shifted alpha particle gyrofrequency, the instabilities arising from this branch can be very efficient in transferring energy to the alpha particles.

We show that the alpha particle branch leads to wave couplings, which generate new decay and modulational instabilities. Some of these instabilities involve alpha sound waves – waves supported essentially by the drifting alpha particles – which can be important in the preferential heating of the alpha particles, as observed in high speed solar wind streams [see Marsch, 1991, and references therein]. We consider also the nonlinear stability of the proton branch (the branch which has the proton resonance) for frequencies much higher than the Alfvén range. This study is motivated by the re-

sults of the linear stability analysis, which shows that the growth rate is important at higher frequencies. Let us note that the scope of the paper is to explore the field and provide a general overview of its potentialities. The detailed study of the physics of each coupling lies beyond its boundaries, and it should be developed in subsequent phases of the research.

The layout of the paper is as follows. In section II the linear theory of the EICW in an electron-proton plasma with minor He⁺ and O⁺ ions is briefly reviewed. In section III the nonlinear dispersion relation for the mode coupling in a characteristic magnetospheric scenario is derived. In section IV the parametric decays of the EICW are analyzed. In section V the linear stability of the circularly polarized waves in a solar wind type plasma is discussed. In section VI the dispersion relation of Hollweg et al. (1993) is briefly reviewed. In section VII the nonlinear stability of the alpha particle branch of the dispersion relation is studied. In section VIII the nonlinear stability of the proton branch is studied for frequencies of the pump wave close to the proton resonance. In section IX we return to the alpha branch to illustrate a number of cases of interest. The results are summarized and discussed in section X.

II. Linear theory of EICW

The dispersion relation of EICW propagating parallel to the external magnetic field in a homogeneous plasma, is given by [see, e.g., Gomberoff 1992]:

$$y_0^2 = \sum_l \left\{ \frac{z_l}{M_l} \eta_{lw} A_l - z_l \eta_{lw} x_0 - \frac{z_l \eta_{lw}}{M_l y_0 \beta_{\parallel l}^{1/2}} Z \left(\frac{M_l x_0 - 1}{M_l y_0 \beta_{\parallel l}^{1/2}} \right) \right. \\ \left. [A_l (1 - M_l x_0) - M_l x_0] \right\} + \sum_l \frac{z_l \eta_{lc} M_l x_0^2}{1 - M_l x_0}. \quad (1)$$

where $y_0 = kv_A/\Omega_p$, $v_A = B_0/(4\pi m_p n_p)^{1/2}$ is the Alfvén velocity, $x_0 = \omega/\Omega_p$, $A_l = (T_{\perp}/T_{\parallel} - 1)_l$, $\beta_{\parallel l} = 8\pi m_p n_{lh} kT_{\parallel l}/m_l B_0^2$, $\eta_{lh} = n_{lh}/n_p$, $\eta_{lc} = n_{lc}/n_p$, z_l is the ion charge, Z is the plasma dispersion function [Fried and Conte, 1961], $M_l = m_l/z_l m_p$, Ω_p is the proton gyrofrequency, $T_{parallel}$, T_{\perp} , are the paral-

lel and perpendicular temperature, l is the index of the ion species, η_{cp} , η_{hp} , are the concentrations of cold and hot protons, respectively and the sum over l is over all plasma components.

Assuming the plasma to be composed of electrons,

protons, He^+ , and O^+ ions, from the real part of Eq. (1) we obtain the cold plasma dispersion relation,

$$y_0^2 = \frac{x_0^2}{1-x_0} + \frac{4\eta_{He^+}x_0^2}{1-4x_0} + \frac{16\eta_{O^+}x_0^2}{1-16x_0}. \quad (2)$$

The dispersion relation given by the last equation is illustrated in Fig. (1) for $\eta_{He^+} = n_{He^+}/n_p = 0.12$, and $\eta_{O^+} = n_{O^+}/n_p = 0.01$. These values are typical of the magnetospheric region to be examined in section IV. The first quadrant corresponds to the left-hand polarized EICW propagating forward along the external magnetic field in the proton rest frame. In this quadrant the dispersion relation has three branches. One which has a resonance at the O^+ ion gyrofrequency (to be called the O branch). Then there is another branch which has a resonance at the He^+ gyrofrequency (He branch). Finally, there is a branch that has a resonance at the proton gyrofrequency (proton branch). The second quadrant in Fig. (1) corresponds to the dispersion relation of right hand polarized waves moving backwards. The third quadrant, having $\omega < 0$ and $k < 0$, describes right hand polarized waves moving forward, and the fourth quadrant corresponds to the dispersion relation of left hand polarized waves moving backwards [Gomberoff et al., 1995b].

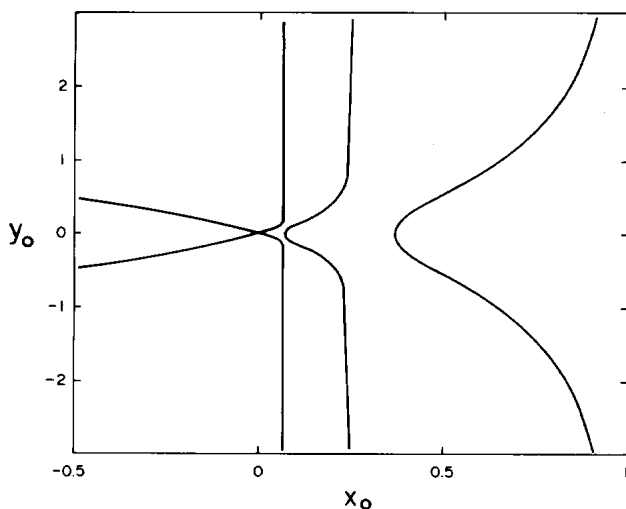


Figure 1. Linear dispersion relation, normalized wavenumber, $y = kv_A/\Omega_p$, vs. normalized frequency, $x = \omega/\Omega_p$, for $\eta_{He^+} = 0.12$, and $\eta_{O^+} = 0.01$.

We shall assume a magnetospheric plasma model consisting of $n_e = 12.3cm^{-3}$, $n_{pc} = 10cm^{-3}$, $n_{ph} = 1.1cm^{-3}$, $n_{He^+} = 1.2cm^{-3}$, $n_{O^+} = 0.1cm^{-3}$, $KT_{pc}/2 \simeq KT_{He^+}/2 \simeq KT_{O^+} = 5eV$, $KT_{ph}/2 = 17keV$, $B_0 = 130nT$, and $A_p = 1$. These values are

consistent with the geostationary region explored by GEOS 1 and 2 [Young et al., 1981].

The growth rates can be calculated from the imaginary part of Eq. (1) assuming that the plasma is composed of Maxwellian electrons, a hot proton component described by a biMaxwellian distribution function with thermal anisotropy A_p [Gomberoff and Neira, 1983; Kozyra et al. 1984; Gomberoff 1992]. In some of the above-mentioned references it is assumed that the thermal components are cold. However, the cold components are, of course, not completely cold, but have thermal energies ranging from a few eV up to 10 eV [D  cr  au et al., 1982; Chappell, 1983]. Thermal effects due to the ‘cold’ components have been studied by Gendrin et. al. [1984], Gomberoff and Vega [1987], and Gomberoff [1992].

It is well known that the proton thermal anisotropy of the minor hot proton component can render unstable the three branches of the dispersion relation, (see Fig. 1), in agreement with observations performed on board the GEOS 1 and 2 satellites [see Young et al., 1981; Roux et al., 1982]. The branch with the resonance at the O^+ ion gyrofrequency is unstable in the region $0 < \omega < \Omega_{O^+}$. The branch having a resonance at the He^+ ion gyrofrequency is unstable in the region $\Omega_{O^+} < \omega_{c1} < \omega < \Omega_{He^+}$, and the branch with the resonance at the proton gyrofrequency is unstable in the region $\omega_{c2} < \omega < \omega_m < \Omega_p$. The frequencies ω_{c1} and ω_{c2} are cutoff frequencies, which depend on the minor ion concentration, and ω_m is the marginal frequency, which for $A_p = 1$ occurs at $\omega_m = \Omega_p/2$ [Gomberoff and Neira, 1983; Kozyra et al., 1984; Gomberoff, 1992].

Having established the fact that the three branches of the dispersion relation, Eq. (2), can be active in the magnetosphere, we shall study the nonlinear stability of each branch in their corresponding excited regions.

To this end, in the next section we derive the nonlinear dispersion relation of the left hand polarized EICW.

III. Nonlinear dispersion relation of the EICW

So far we have used kinetic theory to study the linear properties of the EICW. We shall now assume a fluid description of the plasma. By doing this, important effects like Landau damping and resonance absorption are being left out. Clearly, a detailed study of the

physics of each decay should include these effects [Lee and Kaw, 1972; Inhester, 1990]. However, a fluid model is sufficient to provide a general survey of possible wave couplings and instabilities, which is the purpose of the present paper.

Thus, each plasma component is assumed to satisfy the following fluid equation of motion:

$$\left(\frac{\partial}{\partial t} + \mathbf{u} \cdot \nabla\right)\vec{u} = \frac{q_l}{m_l}\left\{\vec{E} + \frac{1}{c}\vec{u} \times \vec{B}\right\} - \frac{\vec{\nabla}p}{n_l m_l}, \quad (3)$$

where \vec{u} is the bulk velocity, q_l the electric charge, m_l , the mass, \vec{E} and \vec{B} the electric and magnetic field, and p the pressure.

It is well known that in a single ion-component plasma, the EICW are exact solutions of Eqs. (3) [Ferraro, 1955]. A general proof of Ferraro's result for a multicomponent plasma, including drifts among the ion species, can be found in Appendix 1. The magnetospheric plasma considered here corresponds to the case when there is no drift between the ion species. Thus, the circularly polarized EICW in the magnetosphere described by Eq. (3) can have large amplitudes.

We now assume that the background plasma is composed of electrons, cold protons (cp), hot protons (hp), He^+ ions, O^+ ions and by a circularly polarized wave, the pump, which satisfies the dispersion relation given by Eq. (2).

Taking the external magnetic field to be along the z -direction, B_{0z} , we introduce the following pertur-

bations: $\delta u_z = Re[u_{||} exp(ikz - i\omega t)]$, $\delta E_z = Re[\epsilon exp(ikz - i\omega t)]$, $\delta n = Re[\bar{n} exp(ikz - i\omega t)]$, and $\delta p = Re[\bar{p} exp(ikz - i\omega t)]$. The pressure is assumed to behave adiabatically, $\delta p/p_0 = \gamma \delta n/n_0$, where γ is the adiabaticity coefficient. Using the definitions $u_{\perp} = u_x + iu_y$, $B_{\perp} = B_x + iB_y$, and $E_{\perp} = E_x + iE_y$, the perpendicular perturbations are given by $\delta u_{\perp} = v_+ e^{(ik_+z - i\omega_+t)} + v_- e^{(ik_-z - i\omega_-t)}$ and similarly for δB_{\perp} and δE_{\perp} . The problem is now solved using standard linear perturbation theory.

Thus, from the mass conservation equation we obtain:

$$\delta n = n_0 Re\left\{\frac{uk}{\omega} e^{ikz - i\omega t}\right\}, \quad (4)$$

From the (x,y)-component of Eq. (4) it follows:

$$(\omega_c - \omega_+)v_+ = -\frac{q\omega_+ b_+}{mck_+} + \frac{Bq\omega_c u_{||}}{2mc(\omega_c - \omega_0)}, \quad (5)$$

where

$$\delta u_{\perp} = v_+ e^{ik_+z - i\omega_+t} + v_- e^{ik_-z - i\omega_-t}, \quad (6)$$

and similarly for $(\delta B_{\perp}, \delta j_{\perp})$ in terms of (b_{\pm}, j_{\pm}) . The other quantities are $B_{\perp 0} = B exp(ik_0z - i\omega_0t)$ with B real, $\omega_{\pm} = \omega_0 \pm \omega$, $k_{\pm} = k_0 \pm k$, where ω_0 and k_0 are the frequency and wavenumber of the pump wave. An explicit derivation of Eq. (5) is given in section VI.

On the other hand, from the z -component of Eq. (4) we obtain:

$$\left\{1 - \frac{k^2 v_s^2}{\omega^2}\right\} u_{||} = \frac{q}{m\omega} \left\{i\epsilon + \frac{B}{c} \left[\frac{v_{\perp 0}}{B_{\perp 0}}(b_+ - b_-^*) + v_-^* - v_+\right]\right\}, \quad (7)$$

where $u_{||}$ refers to the direction along the external magnetic field, $v_s^2 = \gamma p_0/\rho_0$ is the sound speed of the ion species considered, and ϵ indicates the longitudinal electric field.

Assuming the electrons to be massless, from Eq. (5), its complex conjugate, and Eq. (7), one can solve for the longitudinal component of the electric field, ϵ . We obtain,

$$i\epsilon = \frac{Bb_-^*}{B_{0z}c} \left(\frac{\omega_-^*}{k_-^*} - \frac{\omega_0}{k_0}\right) - \frac{Bb_+}{B_{0z}c} \left(\frac{\omega_+}{k_+} - \frac{\omega_0}{k_0}\right) + \frac{\gamma_e K T_e k^2 u_{||e}}{|e|\omega}. \quad (8)$$

Assuming charge quasi-neutrality, from Eq.(4) it follows,

$$u_{||e} = \sum_l \frac{\eta_l u_{||l}}{1 + \eta_{He^+} + \eta_{O^+}}, \quad (9)$$

where

$$\eta_l = \frac{n_l}{n_{cp} + n_{hp}}, \quad l = cp, hp, He, O, \quad (10)$$

and the electrons can be eliminated altogether.

Thus, for each plasma component, the parallel velocity is given by,

$$\tilde{A}_{cp} \bar{u}_{\parallel cp} = B_p + \beta_e [\eta_{hp} \bar{u}_{\parallel hp} + \eta_{He^+} \bar{u}_{\parallel He^+} + \eta_{O^+} \bar{u}_{O^+}] \quad (11)$$

$$\tilde{A}_{hp} \bar{u}_{\parallel hp} = B_p + \beta_e [\eta_{pc} \bar{u}_{\parallel pc} + \eta_{He^+} \bar{u}_{\parallel He^+} + \eta_{O^+} \bar{u}_{O^+}], \quad (12)$$

$$\tilde{A}_{He^+} \bar{u}_{\parallel He^+} = B_{He^+} + \frac{\beta_e}{4} [\eta_{cp} \bar{u}_{\parallel cp} + \eta_{hp} \bar{u}_{\parallel hp} + \eta_{O^+} \bar{u}_{O^+}], \quad (13)$$

$$\tilde{A}_{O^+} \bar{u}_{\parallel O^+} = B_{O^+} + \frac{\beta_e}{16} [\eta_{cp} \bar{u}_{\parallel cp} + \eta_{hp} \bar{u}_{\parallel hp} + \eta_{He^+} \bar{u}_{He^+}], \quad (14)$$

where

$$\bar{u}_l = \frac{u_l}{v_A} \quad l = cp, hp, He^+, O^+, \quad (15)$$

$$\tilde{A}_l = [1 - (\frac{\beta_l}{m_l/m_p} + \frac{\eta_l \beta_e}{m_l/m_p}) \frac{y^2}{x^2}] + \alpha_l, \quad l = cp, hp, He^+, O^+. \quad (16)$$

$$B_l = \frac{1}{B} (B_l^- b_-^* - B_l^+ b_+), \quad l = p, He, O, \quad (17)$$

$$\alpha_l^\pm = \frac{B^2}{B_{0z}^2} \frac{1}{x} \frac{x_0^2 y_\pm \psi_{\pm(l)} - x_\pm^2 y_0 \psi_{0(l)}}{y_0 y_\pm \psi_{0(l)} \psi_{\pm(l)}}, \quad l = p, He^+, O^+. \quad (18)$$

$$\beta_l = \frac{4\pi(n_{cp} + n_{hp})\gamma_l K T_l}{B_{0z}^2} \quad (l = cp, hp, He^+, O^+), \quad (19)$$

$$\beta_e = \frac{4\pi(n_{cp} + n_{hp})\gamma_e K T_e}{B_{0z}^2 (1 + \eta_{He^+} + \eta_{O^+})}, \quad (20)$$

and

$$x_\pm = x_0 \pm x, \quad (21)$$

$$y_\pm = y_0 \pm y, \quad (22)$$

$$\psi_0 = 1 - x_0, \quad (23)$$

$$\psi_\pm = 1 - x_\pm, \quad (24)$$

$$\psi_{\pm(He^+)} = 1 - 4x_\pm, \quad (25)$$

$$\psi_{\pm(O^+)} = 1 - 16x_\pm, \quad (26)$$

$$\psi_{0(He^+)} = 1 - 4x_0, \quad (27)$$

$$\psi_{0(O^+)} = 1 - 16x_0, \quad (28)$$

On the other hand,

$$\sum_i j_+^i = j_+^e + j_+^p + j_+^{He^+} + j_+^{O^+}, \quad (29)$$

which, due to Ampere's law, $k_+ b_+ = -4\pi \sum j_+/c$, leads to,

$$\sum j_+ = \frac{q(n_{cp} + n_{hp})}{B_{0z}} \left\{ \frac{B}{2} \left[\frac{1}{1-x_0} (x_0 + \frac{x_+}{1-x_+} - \frac{y}{y_0} \frac{x_0^2}{x}) \right] \right. \\ \left. \cdot (\eta_{pc} u_{\parallel pc} + \eta_{ph} u_{\parallel ph}) \right\}$$

$$\begin{aligned}
 & + \frac{4\eta_{He+}}{1-4x_0} \left(x_0 - \frac{y}{y_0} \frac{x_0^2}{x} + \frac{x_+}{1-4x_+}\right) u_{\parallel He+} \\
 & + \frac{16\eta_{O+}}{1-16x_0} \left(x_0 - \frac{yx_0^2}{y_0x} + \frac{x_+}{1-16x_0}\right) u_{\parallel O+} \\
 & - b_+ v_A \frac{x_+}{y_+} \left[\frac{x_+}{1-x_+} + \frac{4\eta_{He+}x_+}{1-4x_+} + \frac{16\eta_{O+}x_+}{1-16x_+}\right].
 \end{aligned} \tag{30}$$

Proceeding in a similar way for $\sum j^*$, one obtains two equations in terms of the parallel velocities, b_-^* , and b_+ ,

$$B[R_+(\eta_{cp} u_{\parallel cp} + \eta_{hp} u_{\parallel hp}) + R_{+(He+)} u_{\parallel He+} + R_{+(O+)} u_{\parallel O+}] + v_A L_+ b_+ = 0, \tag{31}$$

$$B[R_-(\eta_{cp} u_{\parallel cp} + \eta_{hp} u_{\parallel hp}) + R_{-(He+)} u_{\parallel He+} + R_{-(O+)} u_{\parallel O+}] + v_A L_- b_-^* = 0, \tag{32}$$

where

$$L_{\pm} = y_{\pm}^2 - \frac{x_{\pm}^2}{\psi_{\pm}} - \frac{4\eta_{He+}x_{\pm}^2}{\psi_{\pm(He+)}} - \frac{16\eta_{O+}x_{\pm}^2}{\psi_{\pm(O+)}} \tag{33}$$

$$R_{\pm} = y_{\pm} \left(x_0 - \frac{yx_0^2}{y_0x} + \frac{x_{\pm}}{\psi_{\pm}}\right) \frac{1}{2\psi_0}, \tag{34}$$

$$R_{\pm(He+)} = 4\eta_{He+}y_{\pm} \left(x_0 - \frac{yx_0^2}{y_0x} + \frac{x_{\pm}}{\psi_{\pm(He+)}}\right) \frac{1}{2\psi_0(He+)}, \tag{35}$$

$$R_{\pm(O+)} = 16\eta_{O+}y_{\pm} \left(x_0 - \frac{yx_0^2}{y_0x} + \frac{x_{\pm}}{\psi_{\pm(O+)}}\right) \frac{1}{2\psi_0(O+)}. \tag{36}$$

Upon elimination of the parallel velocities using Eqs. (11-14), one finally obtains two equations in terms of b_-^* and b_+ only. Setting the determinant of these equations equal to zero yields the nonlinear dispersion relation.

It is convenient to define the following quantities,

$$Q = 1 - \beta_e \frac{y^2}{x^2} \left(\frac{\eta_{cp}}{A_{cp}} + \frac{\eta_{hp}}{A_{hp}} + \frac{\eta_{He+}}{4A_{He+}} + \frac{\eta_{O+}}{16A_{O+}}\right), \tag{37}$$

$$P_{\pm} = \beta_e y^2 \left(\frac{\eta_{cp}}{A_{pc}} + \frac{\eta_{hp}}{A_{hp}}\right) \bar{R}_{\pm} + \frac{\eta_{He+} \bar{R}_{\pm(He+)}}{4A_{He+}} + \frac{\eta_{O+} \bar{R}_{\pm(O+)}}{16A_{O+}}, \tag{38}$$

and

$$\begin{aligned}
 T_{\pm}^{\pm} &= \alpha_p^{\pm} (\bar{R}_{\pm} Q + P_{\pm}) \left(\frac{\eta_{pc}}{A_{pc}} + \frac{\eta_{ph}}{A_{ph}}\right) + \\
 & \alpha_{He+}^{\pm} \frac{(\bar{R}_{\pm(He+)} Q + \eta_{He+} P_{\pm})}{A_{He+}} + \alpha_{O+}^{\pm} \frac{(\bar{R}_{\pm(O+)} Q + \eta_{O+} P_{\pm})}{A_{O+}},
 \end{aligned} \tag{39}$$

where

$$A_l = 1 - \left(\frac{\beta_l}{m_l/m_p}\right) \frac{y^2}{x^2} + \frac{B^2}{B_{0z}^2} \frac{1}{\psi_{0(l)} \psi_{+(l)} \psi_{-(l)}}, \quad l = cp, hp, He, O. \tag{40}$$

and $\bar{R}_{\pm l} = x R_{\pm l}$ with $l=cp, He, O$.

The dispersion relation can now be written in the following form,

$$L_+ L_- Q + L_+ T_-^- - L_- T_+^+ + \frac{T_+^- T_-^+ - T_+^+ T_-^-}{Q} = 0. \tag{41}$$

Except for the first term in Eq. (41), all other terms vanish for zero pump wave intensity, $A = (B/B_{0z})^2$, where B is the magnetic field of the pump wave, and B_{0z} is the external magnetic field.

Hence, for zero pump wave intensity, the dispersion relation reduces to,

$$L_+ L_- Q = 0, \tag{42}$$

From the last equation, it follows that, for zero pump wave intensity,

$$L_{\pm} = y_{\pm}^2 - \frac{x_{\pm}^2}{1 - x_{\pm}} - \frac{4\eta_{He^+} x_{\pm}^2}{1 - 4x_{\pm}} - \frac{16\eta_{O^+} x_{\pm}^2}{1 - 16x_{\pm}} = 0, \tag{43}$$

and

$$Q = 0. \tag{44}$$

Clearly, $L_{\pm} = 0$ correspond to the circularly polarized waves satisfying the same dispersion relation given by Eq. (2), except that they are now referred to a new origin given by (x_0, y_0) which are the frequency and wavenumber of the pump wave. Note that when $L_{\pm} = 0$, δn , δp , E_z , and δu_z have zero amplitude and Eq. (43) is equivalent to Eq. (2), with $x_0 = y_0 = 0$.

Eq. (44) gives the sounds present in the system. Since the electrons, cold protons, He^+ , and O^+ ions are much colder than the hot protons, $\beta_e, \beta_{cp}, \beta_{He^+}, \beta_{O^+} \ll \beta_{hp}$, the solutions of Eq. (44) are given by:

$$x = \pm(\beta_{cp} + \eta_{cp}\beta_e)^{1/2}y, \tag{45}$$

$$x = \pm(\beta_{hp} + \eta_{hp}\beta_e)^{1/2}y, \tag{46}$$

$$x = \pm\frac{1}{2}(\beta_{He^+} + \eta_{He^+}\beta_e)^{1/2}y, \tag{47}$$

$$x = \pm\frac{1}{4}(\beta_{O^+} + \eta_{O^+}\beta_e)^{1/2}y. \tag{48}$$

Thus, there are eight electro-acoustic modes in the system. The first two, given by Eq. (45), are ordinary sound waves. The second two, given by Eq. (46), are supported essentially by the hot protons, the other two, given by Eq. (47), are supported mainly by the He^+ ions, and the last two, given by Eq. (48) are carried mainly by The O^+ ions.

IV. Parametric decay of the EICW

IV.1 Oxygen Branch

We shall begin by assuming

that the pump wave belongs to the branch of the dispersion relation which has a resonance at the O^+ ion gyrofrequency (see Fig. 1). We choose the frequency of the pump wave to be $x_0 = 0.05$ and the corresponding wavenumber $y_0 = 0.0783$. This frequency value is in the region of ion cyclotron excitation of this branch [Gomberoff and Neira, 1983; Kozyra et al. 1984].

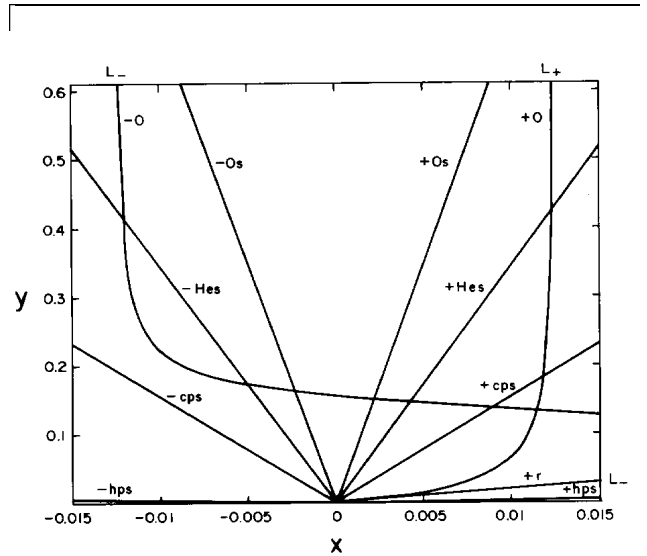


Figure 2. Solution of the dispersion relation, Eq. (48), for zero pump wave intensity, $A = 0$. The position of the pump is $x_0 = 0.05$ and $y_0 = 0.0783$, on the O^+ branch. The other plasma parameters are, $\beta_e = 1.1 \times 10^{-3}$, $\beta_{ph} = 11.36$, $\beta_{pc} = \beta_{He^+} = \beta_{O^+} = 3.3 \times 10^{-3}$, $\eta_{cp} = 0.9$, $\eta_{hp} = 0.1$, and $\eta_{He^+} = 0.12$, and $\eta_{O^+} = 0.01$.

In Fig. (2) we have plotted the dispersion relation, Eq. (41), for zero pump wave intensity. From left to right, the lines correspond to the following solutions of Eq. (42). The $-hps$ sound which corresponds to the negative solution given by Eq. (46). The $-cps$ line, which is the negative solution of Eq. (45). The $-O$ line, which is a solution of $L_- = 0$, and corresponds to the branch which has a resonance at the oxygen gyrofrequency in the fourth quadrant of Fig. (1). The $-Hes$ line, which corresponds to the negative solution given by Eq. (47). The $-Os$ sound which is the negative solution given by Eq. (48). The $+Os$ sound which corresponds to the positive solution of Eq. (48). The $+Hes$ line, solution of Eq. (47). The $+O$ line, corresponding to the branch of the pump wave in the first quadrant of Fig. (1), and it is a solution of $L_+ = 0$. The $+cps$ solution of Eq. (45) The $+r$ line which is a solution of $L_- = 0$, and corresponds to the branch of

the dispersion relation in the third quadrant of Fig. (1). The $+hps$ sound which is the positive solution given by Eq. (46). There are other lines which do not show up in the figure, corresponding to the He and proton branch in the first quadrant of Fig. (1) and the corresponding reflections into the second quadrant of Fig. (2) coming from the fourth quadrant of Fig. (1). Finally, there is another line which is not shown in the figure, which is a solution of L_+ and corresponds to right hand waves propagating backward relative to the external magnetic field in the second quadrant of Fig. (1). Since the dispersion relation, Eq.(41), is a sixteenth-order equation, there must be sixteen lines in all, which is indeed the case.

The crossings between the lines in Fig. (2), are possible wave couplings with the pump wave when this is turned on. From left to right, these crossings are: $(-O, -cps)$, $(-O, -Os)$, $(+Os, -O)$, $(-O, +Hes)$, $(-O, +cps)$, $(+O, -O)$, $(-O, +O)$, $(+Hes, +O)$, and other crossings not shown in the figure. There is also a crossing between $(+O, +r)$ at the origin. Not all these crossings correspond to wave couplings. A necessary condition is that they must satisfy the resonance conditions $n\omega_0 = \omega_1 + \omega_2$, $n=1,2,\dots$, where ω_1 and ω_2 are the frequency of the daughter waves.

The origin in Fig. (2), corresponds to the coordinates of the pump wave (x_0, y_0) on the O^+ branch of the dispersion relation in Fig. (1). In Fig. (2) the solutions of Eq. (42) are shown only in the first and second quadrant in the (x, y) plane. The other two quadrants can be obtained by rotating the plane through an angle of 180° and, therefore, they contain no new information. The search for parametric decays will be carried through as in Hollweg et al. [1993], and Gomberoff et al. [1994a,b], using the method of Longtin and Sonnerup [1986].

In Fig. (3) we have switched on the pump wave. This is done by solving numerically Eq. (41) for $A \neq 0$. For $A = 10^{-4}$, a comparison between Fig. (2) and (3a), shows that at the position of some of the crossings there are now gaps. The gaps along the vertical direction correspond to instabilities. In fact, if a horizontal line is drawn at the position of the gaps, this line will cross only 14 lines, which means that two of the sixteen real roots have become complex conjugate. This is the case of the crossings between $(-O, +Os)$, $(-O, +Hes)$,

$(-O, +cps)$, $(-O, +O)$, and between $(+r, +O)$ at the origin. The gap between $(-O, +Os)$ is a decay instability where the pump decays into a backward propagation EICW, or sideband wave - solution of $L_- = 0$ - and a forward propagating sound daughter wave. The gap between $(-O, +Hes)$ and $(-O, +cps)$ are also decay instabilities. The next gap between $(-O, +O)$ is a decay, essentially electromagnetic, where the pump wave decays into two sideband waves, one solution of $L_- = 0$, and the other solution of $L_+ = 0$. The coupling is due to space charge fluctuations, that do not correspond to a sound wave eigenmode interacting with the EICW [Forslund et al., 1972]. The fourth gap between $(+O, +r)$ is an electromagnetic modulational instability, where none of the lines involved extend to the origin [Longtin and Sonnerup, 1986].

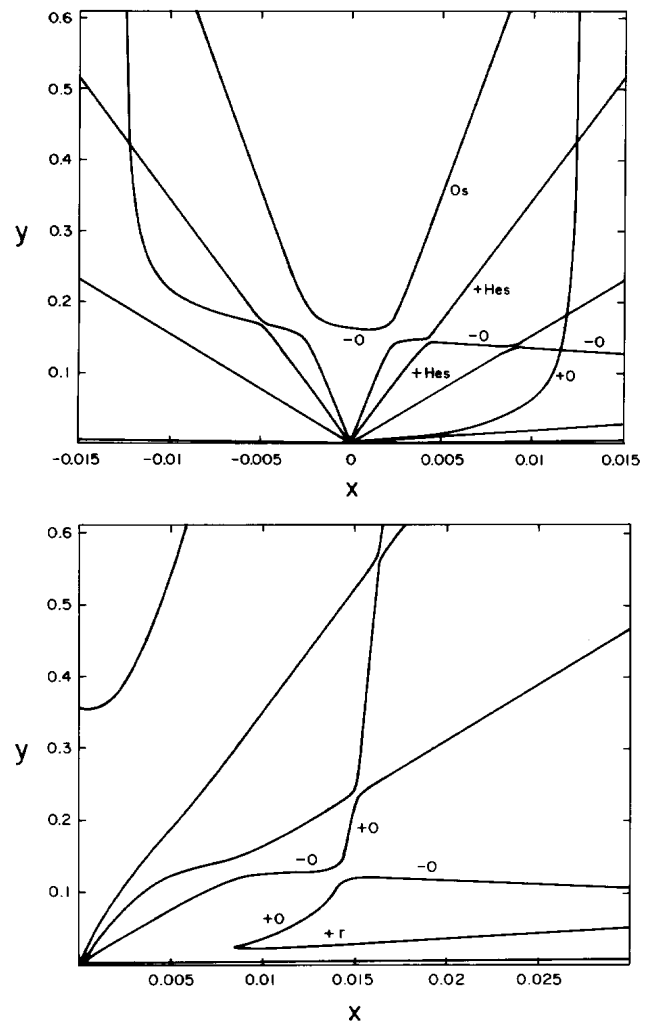


Figure 3. Solution of the dispersion relation, Eq. (48), for (a) $A = 10^{-4}$, and (b) $A = 5 \times 10^{-3}$, showing the two electromagnetic instabilities $(+O, -O)$ and $(+O, +r)$, for the same parameters of Fig. (2).

We have calculated maximum growth/damping rates of some of the crossings. The gaps $(-O, +Os)$ and $(-O, +Hes)$ merge, i. e., they are not separated by a range of y -values with zero growth rate, $\gamma = \omega_i/\Omega_p$. Maximum growth rates, γ_m , however, are separated in each gap. For the gap between $(-O, +Os)$, $\gamma_m = 1.23 \times 10^{-3}$, and occurs at $y=0.1520$, and $x=2.3 \times 10^{-3}$. Similarly, for $(-O, +Hes)$, $\gamma_m = 4.82 \times 10^{-4}$ at $(y=0.1462, x=4.26 \times 10^{-3})$, and for $(-O, +cps)$, $\gamma_m = 6.21 \times 10^{-4}$ at $(y = 0.1375, x = 8.91 \times 10^{-3})$.

In Fig. (3b) the pump wave intensity has been raised to 5×10^{-3} , in order to show the formation of the modulational instability. All of these instabilities are new in the sense that they involve either the sounds supported by the O^+ ions, or/and the branch of the dispersion relation which has the resonance at the O^+ ion gyrofrequency. They can be very efficient in heating up the O^+ ions by Landau damping of the sound waves and/or by resonance absorption. All other crossings in Fig. (2) are avoiding crossings, as it can be seen in Fig. (3b).

IV.2 Helium Branch

We now study the parametric decay of the He branch by taking the pump wave to be one of the waves belonging to the He branch of the dispersion relation given by Eq. (2). For the frequency of the pump wave we choose the value of Fig. (2) of Gomberoff et al. [1994a] i.e., $x_0 = 0.17$. The corresponding y -value is $y_0 = 0.2747$.

Proceeding like in the previous case, in Fig. (4a) we have plotted the solutions of Eq. (41) for zero pump wave intensity. The crossings are essentially the same as those of Fig. (2) of Gomberoff et al. [1995a] except for those involving the Os .

In Fig. (4b), the pump wave intensity has been raised to $A = 10^{-3}$. We can see that there is a new decay instability in which the pump wave decays into a backward propagating left hand EICW, $-He$, and a forward propagating sound wave, $+Os$. The other couplings are similar to Figs. (3) and (4) of Gomberoff et al. [1994a], except for the modulational instability between $(-He, +r)$ which is now between $(-He, +He)$. This is explicitly shown in Fig. (4c).

The maximum growth rate for the case of Fig. (4c),

occurs for the crossing between $(-He, +Hes)$, with $\gamma_m = 2.60 \times 10^{-2}$ at $(y = 0.5440, x = 2.25 \times 10^{-2})$. The electromagnetic instabilities, i. e., the $(+He, -He)$ have $\gamma_m \simeq 10^{-3}$.

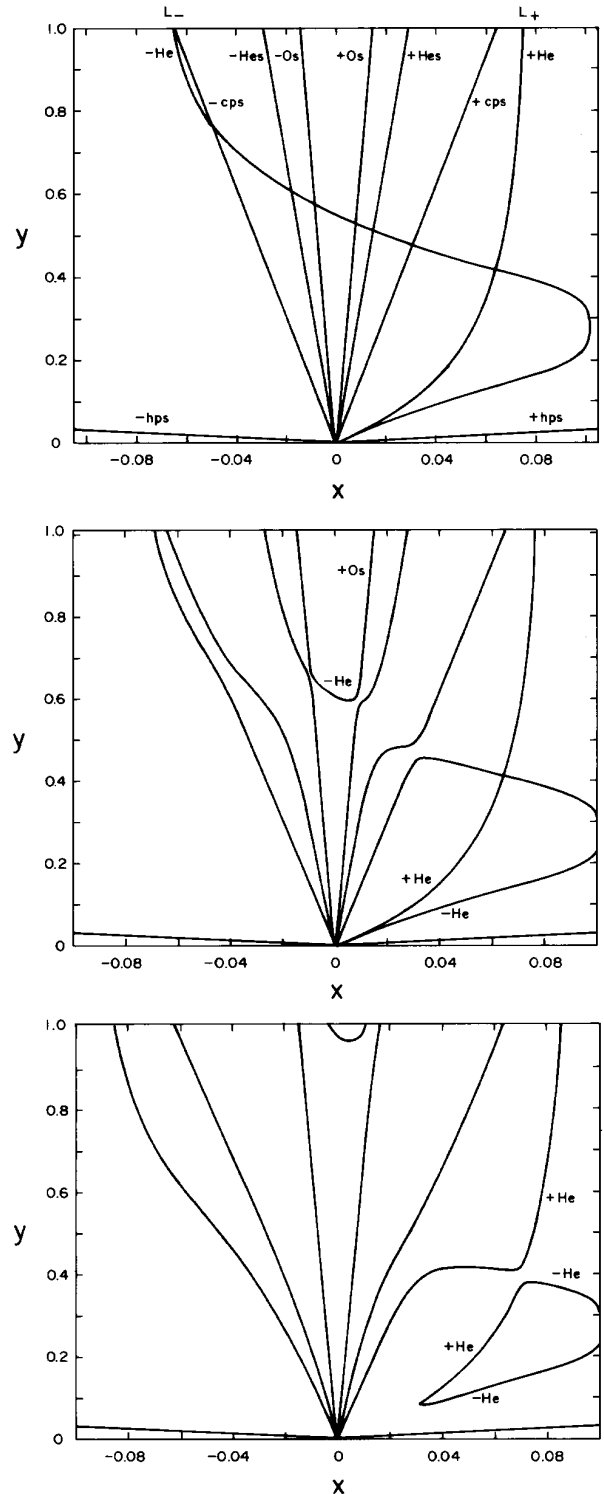


Figure 4. Solution of the dispersion relation, Eq. (48), for the pump wave on the He branch. The frequency and wavenumber of the pump are $x_0 = 0.17$ and $y_0 = 0.2747$ for (a) $A = 0$, (b) $A = 10^{-3}$, and (c) $A = 10^{-2}$. The other parameters are like in Fig. (2).

IV.3 Proton Branch

We choose for the frequency of the pump wave the value $x_0 = 0.4$ like in Gomberoff et al. [1995a]. The corresponding y_0 value is $y_0 = 0.3660$. Fig. (5a) is the dispersion relation given by Eq. (52) for zero pump wave intensity. This situation is very similar to Fig. (9a) of Gomberoff et al. [1994a] except for the new sounds, $\pm Os$. Due to the ($+Os$), there is a new decay instability between ($+Os, -p$) as shown in Fig. (5b) for $A = 10^{-4}$, and in Fig. (5c) for $A = 10^{-3}$. All other crossings are similar to Figs. (9a) and (9b) of Gomberoff et al. [1995a].

$$y^2 = A_p - x - \frac{1}{y\beta_{\parallel p}^{1/2}} Z\left(\frac{x-1}{y\beta_{\parallel p}^{1/2}}\right) [A_p(1-x) - x] - 2\eta(x-yU) - \frac{\eta}{2y\beta_{\parallel \alpha}^{1/2}} Z\left(\frac{2x-2yU-1}{2y\beta_{\parallel \alpha}^{1/2}}\right) [A_\alpha(1-2x+2yU) - 2x+2yU], \tag{49}$$

where $x = \omega/\Omega_p$, $y = kV_A/\Omega_p$, $\Omega_p = qB_0/m_p c$, $U = V_\alpha/V_A$, with V_α the alpha-proton drift velocity and V_A the Alfvén velocity, $\eta = n_\alpha/n_p A_l = T_{\perp l}/T_{\parallel l} - 1$ is the thermal anisotropy of species l , $\beta_{\parallel l} = 8\pi n_p m_p K T_{\parallel l}/m_l B_0^2$, and Z is the plasma dispersion function [Fried and Conte, 1961].

In Figs. (5b) and (5c), maximum growth rates occur for the crossing between ($-p, +Hes$). They are $\gamma_m = 1.11 \times 10^{-2}$ at ($y = 0.690, x = 1.96 \times 10^{-2}$), and $\gamma_m = 3.32 \times 10^{-2}$ at ($y = 74, x = 2.32 \times 10^{-2}$), respectively.

V. Linear analysis of EICW in the fast solar wind

The dispersion relation of the left hand polarized EICW in a plasma composed of electrons, protons and alpha particles drifting relative to the protons is given by [Gomberoff and Elgueta, 1991]:

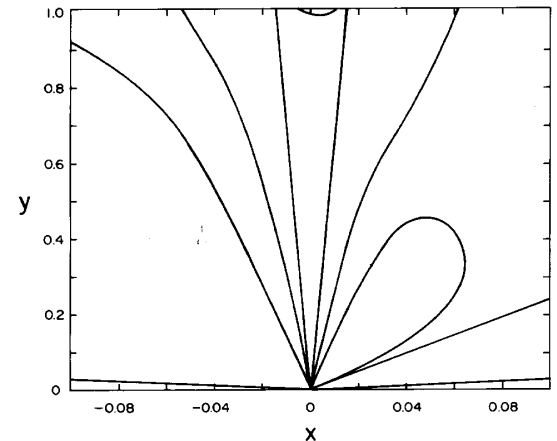
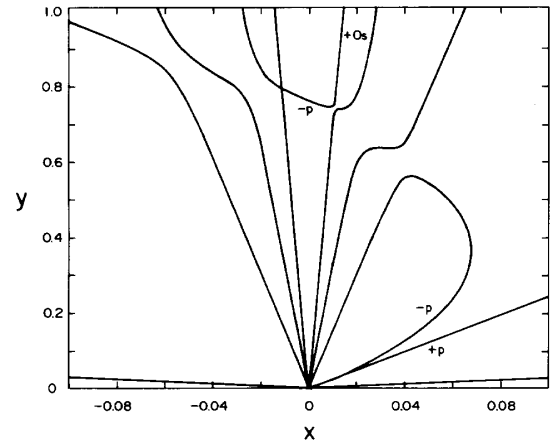
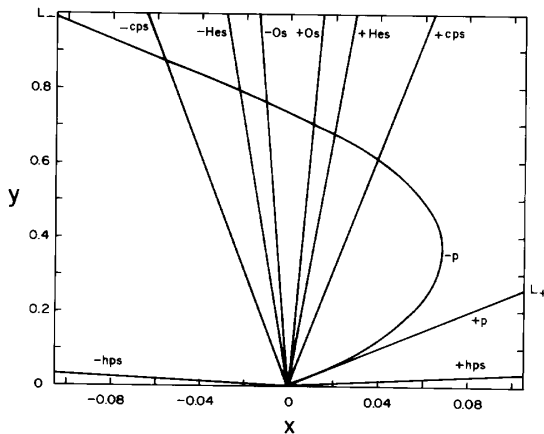


Figure 5. The dispersion relation, Eq. (48), for the pump wave over the proton branch at $x_0 = 0.4$, and $y_0 = 0.3660$, for (a) $A = 0$, (b) $A = 10^{-4}$, and (c) $A = 10^{-3}$. The other parameters are like in Fig. (2).

From the real part of Eq. (49), the cold plasma dispersion relation of the EICW is given by [Gomberoff and Elgueta, 1991]:

$$y^2 = \frac{x^2}{1-x} + \frac{4\eta(x-yU)^2}{1-2x+2yU}. \quad (50)$$

In Fig. 6 the dispersion relation is shown for $U = 0.5$ in the proton rest frame. The first and fourth quadrant describe the forward and backward propagating left hand polarized EICW, respectively. The third and second quadrant describe right hand polarized EICW

propagating forward and backwards, respectively [Hollweg et al., 1993]. The straight line in the first quadrant which reappears in the third quadrant, is due to the drifting alpha particles, and is almost sitting on the Doppler shifted alpha particle gyrofrequency, $(x-yU) \simeq 1/2$.

The growth rate of the waves can be calculated from the imaginary part of Eq. (49). Thus, using the large argument expansion of the Z function, and assuming $\omega = \omega_r + i\omega_i$, with $\omega_i \ll \omega_r$ (to be justified a posteriori), we obtain ($A_\alpha = 0$):

$$\begin{aligned} \gamma = \frac{\omega_i}{\Omega_p} = & \frac{(\pi)^{1/2}}{yF(x,y)} \left\{ \left(\frac{1}{\beta_{\parallel p}}\right)^{1/2} [A_p(1-x) - x] \exp\left(-\frac{(1-x)^2}{y^2\beta_{\parallel p}}\right) \right. \\ & \left. - \left(\frac{1}{\beta_{\parallel \alpha}}\right)^{1/2} \eta(x-yU) \exp\left(-\frac{(2x-2yU-1)^2}{4y^2\beta_{\parallel \alpha}}\right) \right\}, \end{aligned} \quad (51)$$

where

$$F(x,y) = y \left[\frac{x(2-x)}{(1-x)^2} + \frac{8\eta(x-yU)(1-x+yU)}{(1-2x+2yU)^2} \right],$$

and γ is the growth/damping rate normalized to the proton gyrofrequency.

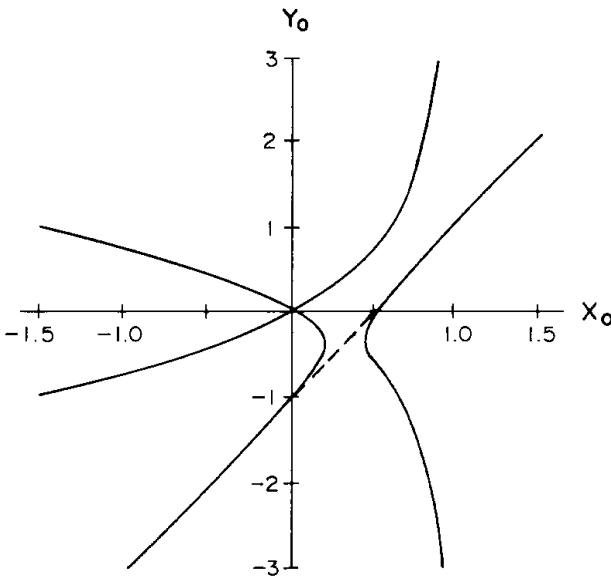


Figure 6. Dispersion relation of the EICW, Eq. (50), for $U = 0.5$.

The approximation we are using fails close to reso-

nance where higher order terms are increasingly important. However, since we are interested in general growth rate trends, the approximation should still hold.

The first term in the right hand side of Eq. (51) is positive between zero and the marginal mode which is given by $x_m = A_p/(A_p + 1)$. The second term in the sum gives the damping of the EICW due to the alpha particles.

One of the properties of high speed solar wind streams is the large values of the thermal anisotropy of the core of the proton distribution function. At heliocentric distances of 0.3 AU values of $A_p = 2 - 4$ are frequently observed (Marsch, 1991).

In Fig. 7 the behaviour of the growth rate is shown for increasing values of the normalized drift velocity, U . The first maximum, corresponding to the proton branch of the dispersion relation (see Figure 1), increases as U increases. On the other hand, the second maximum of the growth rate, which corresponds to the alpha branch of the dispersion relation, decreases as U increases until it becomes negative for $U > 0.3$. This is simple

to understand. In fact, as U increases, this branch of the dispersion relation approaches more and more the Doppler shifted alpha particle resonance and, therefore, it becomes strongly damped due to resonance absorption.

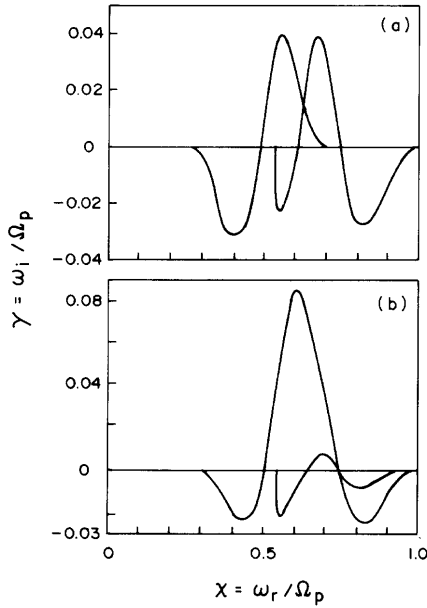


Figure 7. Growth rates of the left hand polarized EICW for $A_p = 3$, $\beta_{\parallel p, \alpha} = 0.1$, and (a) $U = 0.1$, (b) $U = 0.2$.

In Fig. 8 we display the behaviour of the growth rate for a larger value of the thermal anisotropy, $A_p = 5$. A comparison between Figs. 7a and 8a shows that while the maximum growth rate of both branches of the dispersion relation increases, the growth rate of the second branch becomes larger than that of the first branch. As U increases the second branch is completely stabilized, like in the previous case, but now at larger values of the drift velocity, $U > 0.5$. The maximum growth rate of the proton branch increases as U increases, and since it becomes of the order of the real part of the frequency, violating the assumption that $\omega_i \ll \omega_r$, we have omitted this branch in Figs. 7b and 7c.

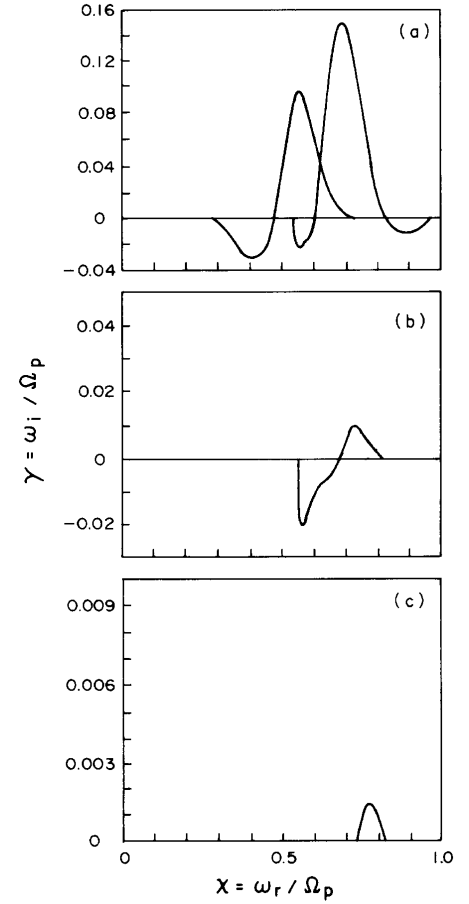


Figure 8. Same as Fig. (7) for $A_p = 5$ and (a) $U = 0.1$, (b) $U = 0.3$ and (c) $U = 0.5$.

Thus, it is clear that both branches of the dispersion relation can be excited in the solar wind, although the alpha particle branch is stabilized at lower values of the alpha-proton drift velocity.

Hollweg et al. (1993), explored the parametric instabilities of the proton branch of the dispersion relation for frequency values of the pump wave close to the origin. However, according to our study of the linear stability of the EICW, maximum growth rates for values of $A_p = 2 - 4$, occur at much larger values of the frequency.

Thus, in the following sections we explore the parametric instabilities of both branches of the dispersion relation, using for the pump wave frequency values dictated by the linear stability analysis.

VI. The dispersion relation

The equation of motion of each plasma species is

$$\left(\frac{\partial}{\partial t} + \vec{v}^l \cdot \nabla\right) \vec{v}^l = \frac{q^l}{m_l} \left(\vec{E} + \frac{\vec{v}^l \times \vec{B}}{c}\right) - \frac{\vec{\nabla} p^l}{m_l n_l}, \quad (52)$$

where \vec{v}^l is the bulk velocity of species l , \vec{E} and \vec{B} are the electric and magnetic field, q^l is the charge of species l , m_l the mass of species l , n_l the particle number density for species l , p^l is the pressure of each species, and c is the speed of light.

Note that the dispersion relation given by Eq. (50) was first derived by using first order perturbation theory of Vlasov's equation [Gomberoff and Elgueta, 1991]. However, it is an exact solution of the set of Eqs. (50) in a cold plasma (see Appendix 1).

We now follow the procedure of Hollweg et al. [1993], in order to study the parametric instabilities of the EICW. Thus, applying first order perturbation theory to the background plasma which consists now of electrons, protons, alpha particles and the circularly polarized waves, i.e.,

$$\begin{aligned} v_{\parallel} &= V_0^{\alpha} + \delta v_{\parallel}, \\ v_{\perp} &= V_{\perp}^p + \delta v_{\perp}, \end{aligned}$$

where

$$\begin{aligned} V_{\perp}^p &= V_{\perp} e^{i(k_0 z - \omega_0 t)}, \\ B_{\perp}^p &= B e^{i(k_0 z - \omega_0 t)}, \\ E_{\perp}^p &= E_{\perp} e^{i(k_0 z - \omega_0 t)}, \end{aligned}$$

are the velocity, magnetic field, and electric field due to the pump wave.

For the perturbations we have,

$$\begin{aligned} \delta v_{\parallel} &= \text{Re}[v_{\parallel} e^{i(kz - \omega t)}], \\ \delta v_{\perp} &= v_+ e^{i(k_+ z - \omega_+ t)} + v_- e^{i(k_- z - \omega_- t)}, \\ \delta b_{\perp} &= b_+ e^{i(k_+ z - \omega_+ t)} + b_- e^{i(k_- z - \omega_- t)}, \\ \delta e_{\perp} &= \epsilon_+ e^{i(k_+ z - \omega_+ t)} + \epsilon_- e^{i(k_- z - \omega_- t)}, \\ \delta e_{\parallel} &= \text{Re}[\epsilon e^{i(kz - \omega t)}]. \end{aligned}$$

Let us now calculate δv_{\perp} from Eq. (52),

$$\frac{d\delta v_{\perp}}{dt} = \frac{q}{m} [\delta e_{\perp} - \frac{i}{c} \delta v_{\perp} B_{0z} + \frac{i}{2c} (\delta v_{\parallel}^* B + \delta v_{\parallel} B) - \frac{i}{c} V_0^{\alpha} \delta b_{\perp}],$$

which, upon using the previous equations, reduces to

$$\begin{aligned} &\frac{\partial}{\partial t} (v_+ e^{i(k_+ z - \omega_+ t)} + v_- e^{i(k_- z - \omega_- t)}) + \\ &\frac{1}{2} (v_{\parallel} e^{i(kz - \omega t)} + v_{\parallel}^* e^{-i(kz - \omega t)}) \frac{\partial}{\partial z} V_{\perp}^p e^{i(k_0 z - \omega_0 t)} = \\ &\frac{q}{m} (\epsilon_+ e^{i(k_+ z - \omega_+ t)} + \epsilon_- e^{i(k_- z - \omega_- t)}) - \\ &\frac{iq}{mc} B_{0z} (v_+ e^{i(k_+ z - \omega_+ t)} + v_- e^{i(k_- z - \omega_- t)}) + \\ &\frac{iq}{mc} B (v_{\parallel} e^{i(kz - \omega t)} + v_{\parallel}^* e^{-i(kz - \omega t)}) e^{i(k_0 z - \omega_0 t)} - \\ &\frac{iq}{mc} V_0^{\alpha} (b_+ e^{i(k_+ z - \omega_+ t)} + b_- e^{i(k_- z - \omega_- t)}), \end{aligned}$$

Multiplying this equation by $e^{-i(k_+ z - \omega_+ t)}$, and averaging over time yields,

$$-i(\omega_c - \omega'_+) v_+ + \frac{i}{2} k_0 V_{\perp}^p v_{\parallel} = \frac{q}{m} \epsilon_+ - \frac{iq}{2mc} B v_{\parallel} - \frac{iq}{mc} V_0^{\alpha} b_+.$$

The last equation can be written in the following form by using Faraday's law, $\nabla \epsilon_+ = -(1/c)(\partial b_+)/(\partial t)$,

$$\epsilon_+ = -b_+ \omega_+ / k_+ c,$$

$$(\omega_c - \omega'_+) v_+ = -\frac{qb_+ \omega'_+}{mc k_+} + \frac{qB}{2mc} \frac{v_{\parallel}}{\omega_c - \omega'_+}.$$

where,

$$\omega'_+ = \omega_+ - k_+ V_0^{\alpha}.$$

and the other quantities are defined in Appendix 2.

Following a similar procedure to the one used in section 3, the nonlinear dispersion relation can be calculated. The result is [Hollweg et al., 1993],

$$L_+L_-D + L_+R_-B_{cc} + L_+R_{-\alpha}B_{cc\alpha} + L_-R_+B_+ + L_-R_\alpha B_\alpha + (B_{cc}B_\alpha - B_{-cc\alpha}B_+)(R_-R_\alpha - R_{-\alpha}R_+)/D = 0 \quad (53)$$

where the various terms are defined in Appendix 2.

The position of the pump is characterized by the coordinates x_0 and y_0 . For zero pump intensity Eq. (53) reduces to $L_+L_-D = 0$. Therefore,

$$L_\pm = (y_\pm)^2 - \frac{x_\pm^2}{1 - x_\pm} - \frac{4\eta(x_\pm - Uy_\pm)^2}{1 - 2(x_\pm - Uy_\pm)} = 0, \quad (54)$$

or

$$D = 0, \quad (55)$$

where $x_\pm = x_0 \pm x$ and $y_\pm = y_0 \pm y$.

Eqs. (54) correspond to the dispersion relation of the circularly polarized waves centered at (x_0, y_0) . The other equation, Eq. (55), corresponds to the sounds present in the system which, for $\eta \ll 1$, are given by,

$$x = \pm(\beta_\epsilon + \beta_p)^{1/2}y, \quad (56)$$

and

$$(x - yU) = \pm(\beta_\alpha)^{1/2}y/2, \quad (57)$$

where $\beta_l = 4\pi n_p \gamma K T_l / B_0^2$ ($l = \epsilon, p, \alpha$).

Eq. (8) is the ordinary sound wave propagating forward and backward relative to the protons. The second equation, Eq. (57), describes the forward and backward propagating alpha sound (in the alpha frame).

The solutions of Eqs. (54) with respect to the new origin, which is now at (x_0, y_0) , give the various branches of the dispersion relation. The crossings between the solutions give the position of the possible wave couplings in the system.

It is interesting to note that if the pump wave is located at (x_0, y_0) on any of the two branches given by the dispersion relation described by Eq. (50), the solutions of Eqs. (54) and (55) are invariant under a rotation through an angle of 180° . Thus, it is sufficient to analyze the solutions in the first and second quad-

rants. Therefore, it is enough to analyze the problem in these quadrants.

It is also important to point out that not all crossings will produce instabilities: only intersections which conserve energy can lead to parametric decays. Sometimes, even an energetically allowed crossing does not lead to instability. The presence of instabilities is characterized by the formation of gaps at the crossing points when the pump is switched on. On the other hand, there are cases denominated avoiding crossings, where the lines separate without forming gaps. Clearly, the latter do not lead to instability. The reason is simple to understand. If an horizontal line is drawn at any value of y , that line must cross as many lines as the order of the dispersion equation. If there are less crossings, it means that two or more roots have become complex conjugate and, therefore, there is a region of instability.

VII. Nonlinear stability of the alpha branch

We begin by exploring the alpha branch of the dispersion relation shown in Fig. 6. We shall assume that the alpha-proton drift velocity is equal to $0.5 V_A$, $A_p = 3$, $\eta = 0.04$ and $\beta_{\parallel p} = 0.1$. These values are consistent with high speed solar wind streams at 0.3 AU.

According to Fig. 8c, a typical value for the frequency of the pump wave can be chosen as $x_0 = 0.73$

with a corresponding wave number $y_0 = 0.436501$. Taking for the interplanetary magnetic field, $B_{0x} = 45 \times 10^{-5}G$, a typical value at 0.3 AU, the frequency and wavelength associated to x_0 and y_0 are $\omega_0 = 3Hz$ and $\lambda_0 = 190km$, respectively. Other parameters are $\beta_e = 0.015$, $\beta_p = 0.15$, and $\beta_\alpha = 0.2$.

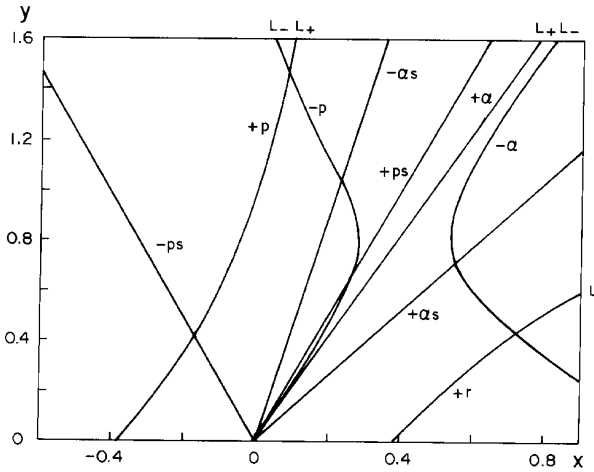


Figure 9. Dispersion relation, Eq. (53), for zero pump wave intensity, $A = 0$. The position of the pump is $x_0 = 0.73$ and $y_0 = 0.436501$. The other parameters are $\beta_e = 0.015$, $\beta_p = 0.15$, $\beta_\alpha = 0.2$, $U = 0.5$, $\eta = 0.04$.

In Fig. 9 we show the dispersion relation, Eq. (53), for zero intensity of the pump wave, $A = (B/B_0)^2 = 0$, and for the position of the pump discussed in the previous paragraph. The straight lines are, from left to right, the backward propagating proton sound $-ps$, the backward propagating alpha sound $-\alpha s$, the forward propagating proton sound $+ps$, and the forward propagating alpha sound $+\alpha s$. The other lines are, from left to right, a solution of $L_+ = 0$ which corresponds to the upper branch of the first quadrant of Fig. (6), the branch which has a resonance at the proton gyrofrequency, and we shall denote it by $+p$. The next curve is a solution of $L_- = 0$ which corresponds to the backward propagating EICW in the fourth quadrant of Fig. (6), namely the branch which has a resonance at the proton gyrofrequency $-p$. The next line is the branch of the pump which is very close to the alpha resonance, is forward propagating and we shall call it $+\alpha$. The next line is a solution of $L_- = 0$ and corresponds to the line which starts in the second quadrant of Fig. (6), crosses the origin into the fourth quadrant and goes to the alpha resonance in the third quadrant. We call this line $-\alpha$. The remaining line is a solution of $L_- = 0$ and corresponds to the upper branch in the third quadrant of Fig. (6). We shall call it $+r$, be-

cause it is a right hand polarized EICW propagating forward. Finally, not shown in the picture, far to the left lies a solution of $L_+ = 0$, a backward propagating EICW corresponding to the segment above y_0 in the second quadrant of Fig. (6). We shall call it $-r$, because it is a right hand polarized EICW, propagating backwards.

The first intersection from the left in Fig. 9 corresponds to a crossing between $(+p, -ps)$. The second crossing is between $(+p, -p)$. The third one is $(-\alpha s, -p)$. The fourth crossing is $(+ps, -p)$. There is a fifth crossing at the origin $(-p, +\alpha)$. In the center to the right of the figure, there is a sixth crossing $(-\alpha, +\alpha s)$ and finally, there is a seventh crossing $(+r, -\alpha)$.

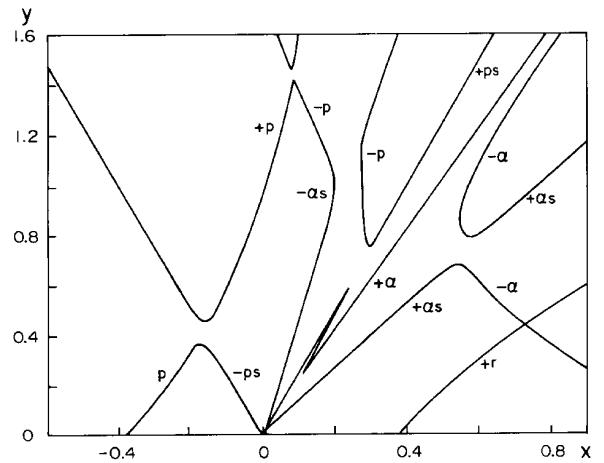


Figure 10. Same as Fig. (9) but for $A = 10^{-4}$.

In order to study possible instabilities we show in Fig. 10 the same situation as in Fig. 9, but for $A = 10^{-4}$. We see that at the place where there was a crossing between $(+p, -ps)$ there is now a gap. This gap is the well known decay instability discussed by many authors. The second gap in the figure (from the left) is due to the second crossing in Fig. (9), the one involving $(+p, -p)$. This is a beat wave instability and is essentially electromagnetic. It was first discussed by Forslund et al. [1972], in an electron-proton plasma [see also Wong and Goldstein, 1986], and by Hollweg et al. [1993], in a three-component plasma. Notice that although it involves only EICW, it is due to electrostatic perturbations. At the position where there was a crossing between $(-\alpha s, -p)$, there is now an avoiding crossing.

Let us take this example to make a brief comment, which can be extended to other cases. We note that

the $-p$ wave belongs to the L_- branch, so that its frequency is $\omega_0 - \omega$, while the $-\alpha s$ sound has a frequency $-\omega$, since it propagate backwards. Clearly, a decay cannot be expected at this crossing because the energy of the quanta, $\omega \neq (\omega_0 - \omega) + (-\omega)$, is not conserved.

The fourth crossing in Fig. 9, $(+ps, -p)$, gives rise to the third gap in Fig. 10. This is a decay instability involving the ordinary sound and a backward propagating left hand polarized EICW. The crossing at the origin, $(-p, +\alpha)$, gives rise to the fourth gap in Fig. 10. This instability is a new instability, which is mainly electromagnetic. Since neither $-p$ nor $+\alpha$ extend to the origin, this corresponds to a modulational instability [see Longtin and Sonnerup, 1986]. The next gap corresponds to a new decay instability corresponding to $(+\alpha s, -\alpha)$. Since this instability involves the $+\alpha$ sound, it can be very efficient in transferring energy to the alpha particles via Landau damping. The last crossing in Fig. 9, $(+r, -\alpha)$, is an avoiding crossing.

Figs. 11a, 11b, 11c, are an enlarged view of the region close to the origin, showing the formation of the modulational instability, for $A = 0$, $A = 10^{-5}$, and $A = 10^{-4}$, respectively.

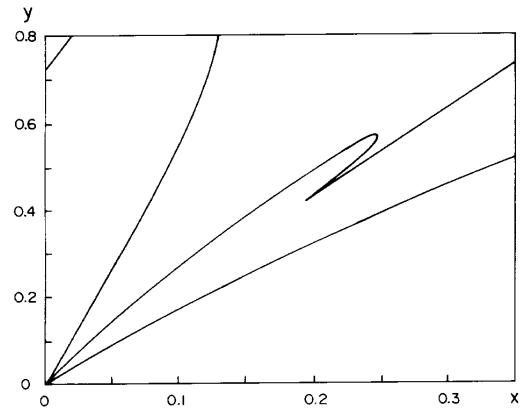
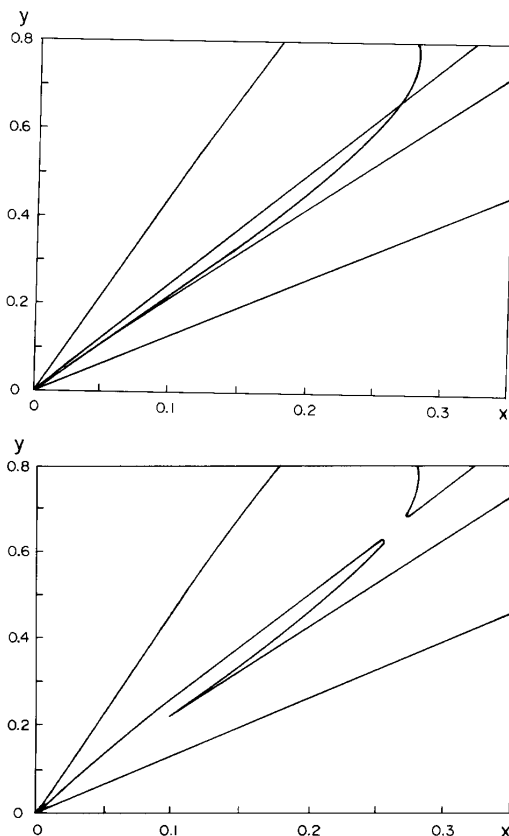


Figure 11. Enlarged view of the origin of Fig. (9) showing the formation of the modulational instability for (a) $A = 0$, (b) $A = 10^{-5}$, and (c) $A = 10^{-4}$.

We now study the effect of decreasing β values. To this end, in Fig. 12 we show the dispersion relation, Eq. (53), for the same position of the pump as in Fig. 9 with $A = 0$ and $\beta_e = \beta_p = \beta_\alpha = 0.03125$. The main difference with Fig. 9 is that $(+ps)$ has exchanged position with $-\alpha s$. As a result, the third crossing, between the $(-p, +ps)$, is now a decay, while the fourth crossing between $(-p, -\alpha s)$ is an avoiding crossing. When the pump is turned on, Figure 8, the avoiding crossing between the $(-p, +\alpha s)$ forces a separation between the two curves, leading to a coupling between $(-\alpha s, +\alpha)$. This crossing generates the gap shown by an arrow in Fig. 13. This is a new modulational instability which involves the pump wave at the alpha branch and a backward propagating alpha sound. This instability can also be very efficient in transferring energy from the pump to the alpha particles by means of Landau damping.

VIII. Nonlinear stability of the proton branch

We now investigate the parametric decay of the proton branch. We choose for the pump wave $x_0 = 0.74$ and $y_0 = 1.4512$. The corresponding frequency and wavelength are $\omega_0 = 2.67Hz$ and $\lambda_0 = 100km$, respectively. We have chosen this value because it is close to the proton resonance, and according to Eq. (51, for $\beta_{\parallel p} = 0.1$, the growth rate is still significant, $\gamma = 2.8 \times 10^{-3}$.

In Fig. 14 we illustrate this situation for $A = 0$, $\beta_e = 0.015$, $\beta_p = 0.15$, and $\beta_\alpha = 0.3$, and $A_p = 3$. We see that, starting from the left, there is a crossing

between $(-p, -ps)$. Then there are two crossings along the $+p$ line with the $-p$ line. Along the $+ps$ line there are three crossings. One at the origin with $+r$ (which is a solution of $L_- = 0$) and a second one at $x = 0.4$ and $y = 1.1$ with $+r$. The third one is $(+ps, -\alpha)$. There is another crossing between $+r$ and $-\alpha$ which, being both solutions of $L_- = 0$, is an avoiding crossing. Then there are four crossings between the $-\alpha$ wave with the $+ps$, $+r$, $+\alpha s$, and $+\alpha$. Finally, there are three new crossings in the upper right part of the figure, $(+\alpha, +\alpha s)$, the $(+\alpha, +r)$, and $(+\alpha s, +r)$.

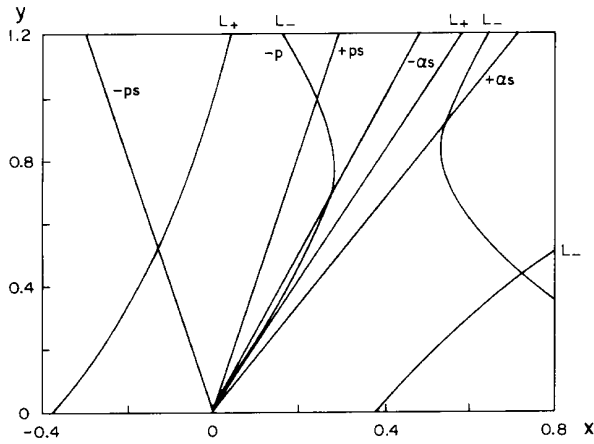


Figure 12. Dispersion relation for zero pump intensity, $A = 0$, with $x_0 = 0.73$ and $y_0 = 0.436501$ with $\eta = 0.04$ and $U = 0.5$ as in Fig. (9), but for $\beta_l = 0.03125$, $l = e, p, \alpha$.

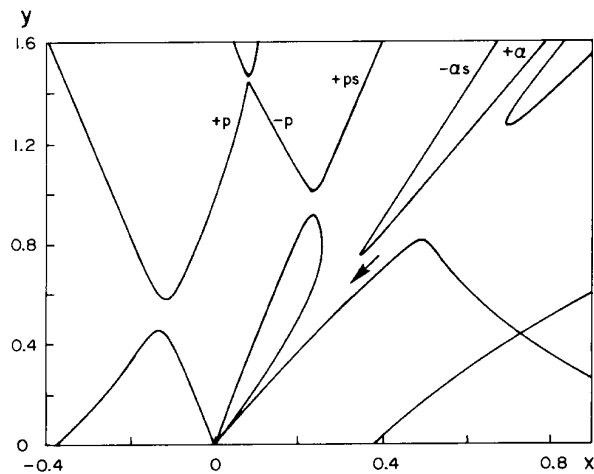


Figure 13. Same as Fig. (12) for $A = 10^{-4}$. The arrow indicates the new modulational instability (see text).

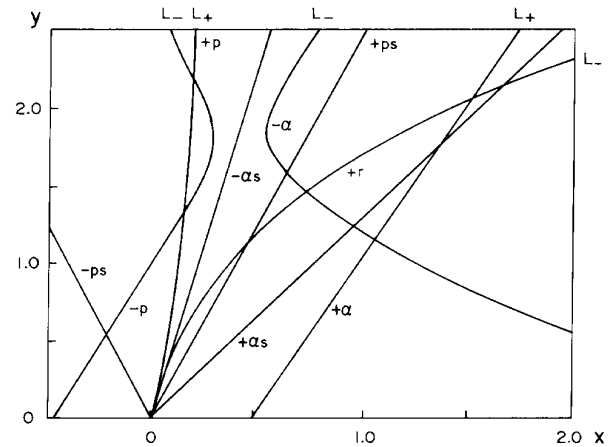


Figure 14. Dispersion relation for zero pump intensity, $A = 0$, for $x_0 = 0.74$, $y_0 = 1.4512$, on the proton branch. The other parameters are $\beta_e = 0.015$, $\beta_p = 0.15$, $\beta_\alpha = 0.2$, $U = 0.5$, $\eta = 0.04$, as in Fig. (9).

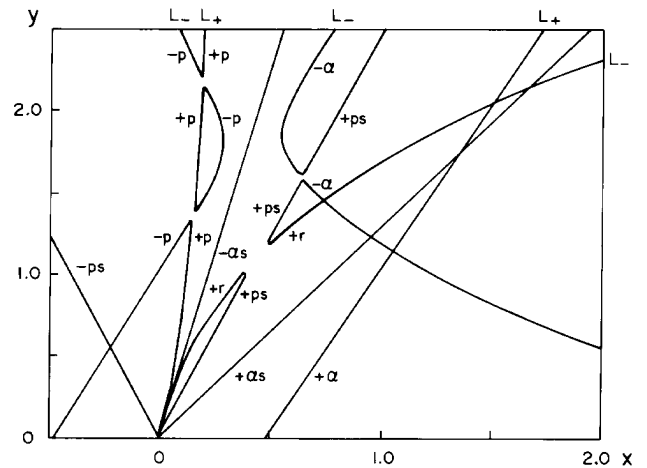


Figure 15. Same as Fig. (14) for $A = 10^{-4}$.

Fig. 15 is the same as Fig. 14, but the intensity of the pump wave has been increased to $A = 10^{-4}$. A comparison between the two figures shows that at the first crossing, in the left part of the figure, there is no coupling, as expected because it is energetically forbidden. Then the two crossings along the $+p$ line give rise to two instabilities which are mainly electromagnetic. The crossing, $(+r, +ps)$, gives rise to a gap corresponding to a decay instability. There is another decay instability between the $(+ps, -\alpha)$. The three crossings in the upper right corner are avoiding crossings. The remaining two crossings $(-\alpha, +\alpha s)$ and $(-\alpha, +\alpha)$ do not show coupling effects.

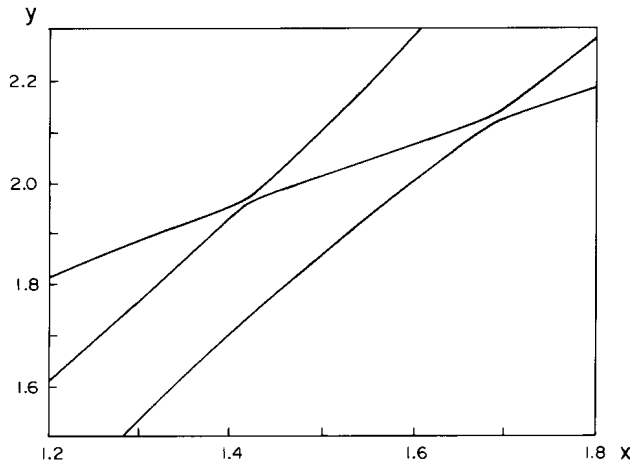


Figure 16. Enlarged view of the upper right part of Fig. (14) for $A = 10^{-4}$, showing that the crossings between $(+r, +\alpha s)$ and $(+r, +\alpha)$ are avoiding crossings.

Fig. 16 is an enlarged view of the upper right part of the last figure, the region involving the crossings $(+\alpha, +r)$ and $(+\alpha s, +r)$. It is clear that these crossings are avoiding. In Fig. 17 we show that the crossing $(+\alpha s, +\alpha)$ is also avoiding.

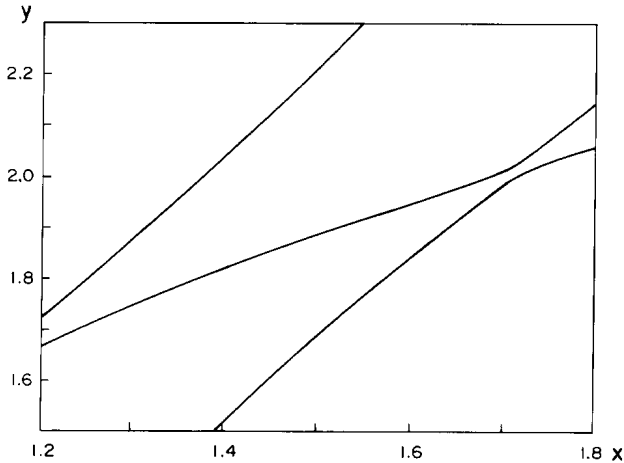


Figure 17. Same as Fig. (14) for $A = 10^{-4}$, showing that $(+\alpha s, +\alpha)$ is an avoiding crossing.

We now reduce the β values to $\beta_l = 0.03125$ with $l = e, p, \alpha$. For $A = 0$ this situation is illustrated in Fig. 18. In Fig. 19 the pump is $A = 10^{-4}$. This case is similar to the previous one, except that due to the interchange between $-\alpha s$ and $+ps$ there is now a modulational instability between the $+ps$ wave and the $+r$ wave at the origin. As before, there are two electromagnetic instabilities along the $+p$ line. Finally, at larger pump intensities, $A \approx 1.2 \times 10^{-2}$, there is a new decay instability (see Fig. 19b) due to the action of the pump on the $+ps$ and $-\alpha$ lines, which tend to coalesce.

This effect is a pump induced coupling because there is no crossing for $A = 0$. To the best of our knowledge, this effect has not been reported before. The modulational instability $(+ps, +r)$ and the decay instability $(+ps, -\alpha)$ are separated by a stable y interval, which shrinks to zero for higher values of the pump.

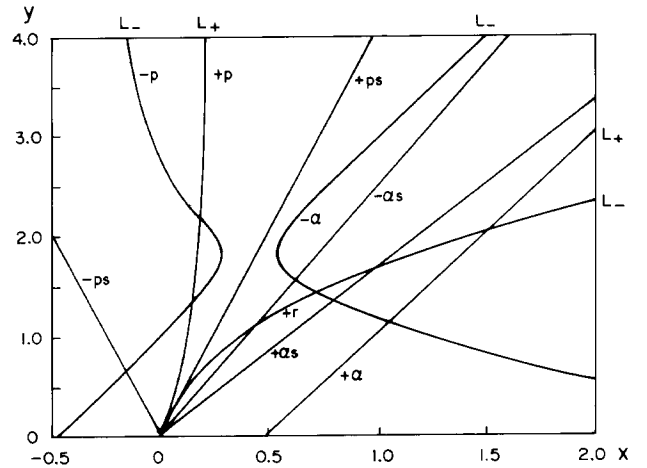


Figure 18. Same as Fig. (14) (pump on the proton branch), but for $\beta_l = 0.03125, l = e, p, \alpha$.

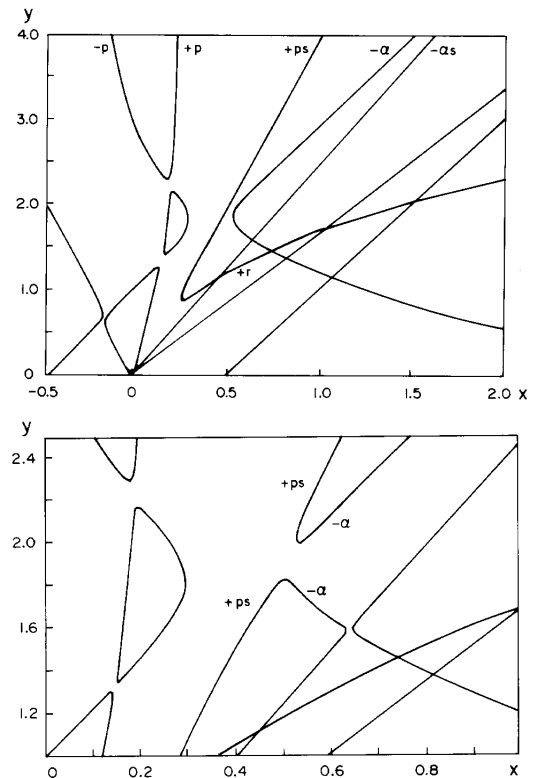


Figure 19. Same as Fig. (18), for (a) $A = 10^{-4}$, (b) $A = 1.4 \times 10^{-2}$, showing the pump induced coupling (see text).

IX. The alpha branch at a lower frequency

In this section we return to the alpha branch, but this time the pump is placed at a lower position, namely at $x_0 = 0.635$ and $y_0 = 0.22879$. We do this for three reasons. First, we want to show that the situation is not too different to the one encountered when the pump wave was at a higher frequency. Second, in order to show that the system is unstable even without the pump wave when the phase velocities of the $+ps$ and the $-\alpha s$ waves are close to each other. Third, to illustrate a case where the presence of a sound wave can interfere with an electromagnetic instability.

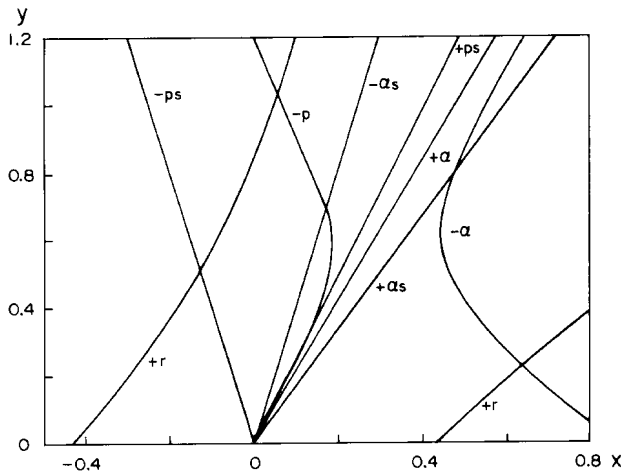


Figure 20. Dispersion relation for zero pump intensity, $A = 0$ (alpha branch) for $x_0 = 0.635, y_0 = 0.22879$. The other parameters are $\beta_e = 0.015, \beta_p = 0.15, \beta_\alpha = 0.2, U = 0.5, \eta = 0.04$, as in Fig. (9).

Fig. 20, where $A = 0$, is the equivalent of Fig. 12 for the new position of the pump. One can see that the nature of the crossings is the same. When the pump is turned on, they give rise to the same gaps shown in Fig. 13.

We now set $\beta_e = \beta_p = \beta_\alpha = 0.08$. Fig. 21 shows the solution of Eq. (53) for zero pump wave intensity. We see that the $+ps$ and the $-\alpha s$ are missing. This is because U is in the range found by Hollweg et al. (1993) where a linear beam-plasma instability occurs due to the overlapping of the two sounds. One interesting point, discussed by Hollweg et al. (1993), is that this instability can be stabilized by the pump wave. In fact, Fig. 22, which is the equivalent of Fig. 21, but for $A = 10^{-2}$, shows that the $+ps$ and $-\alpha s$ have reappeared, due to the action of the pump which has separated the otherwise overlapping sounds. Thus,

waves belonging to the alpha branch can also stabilize the linear beam-plasma instability.

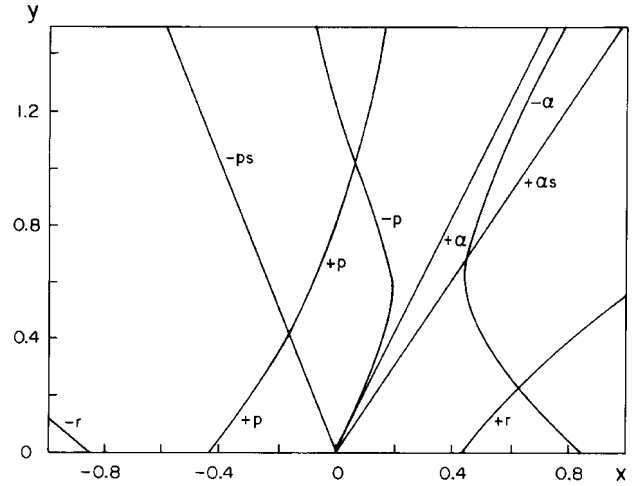


Figure 21. Same as Fig. (20) but $\beta_e = \beta_p = \beta_\alpha = 0.08, l = e, p, \alpha$. Note that $-\alpha s$ and $+ps$ have disappeared.

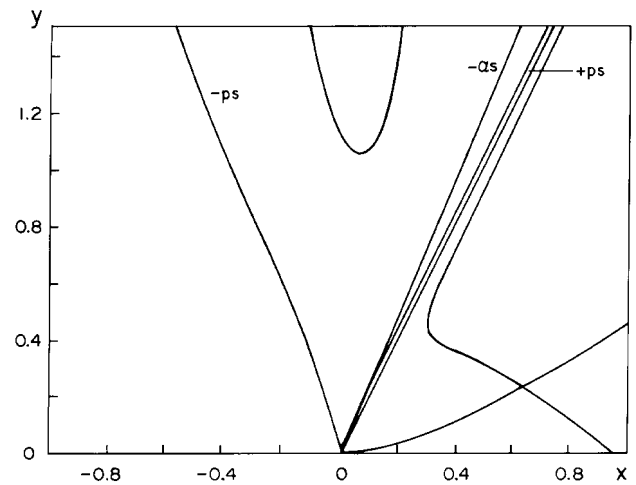


Figure 22. Same as Fig. (21) for $A = 10^{-2}$ showing the reappearance of $-\alpha s$ and $+ps$.

Finally, we take $\beta_e = \beta_p = 0.08$ and $\beta_\alpha = 0.8$. The dispersion relation for $A = 0$ is shown in Fig. 23. We see that the $-\alpha s$ passes through the crossing between the $-p$ and $+p$ waves. This crossing gave rise to an electromagnetic instability in all previous cases. Now, however, due to the presence of the $-\alpha s$, there is a decay instability between the $+p$ and the $-\alpha s$ which has eliminated the $(-p, +p)$ electromagnetic decay. This situation is illustrated in Fig. 24 for a pump wave intensity of $A = 10^{-4}$. Comparing the gap widths of the electromagnetic instability $(+p, -p)$ of Fig. 10, and the electrostatic instability $(+p, -\alpha s)$ of Figure 24, for the same pump wave intensity $A = 10^{-4}$, we see that the

electrostatic coupling is more sensitive to the growth of A : It spreads over a wider range of y values. In fact, it can be shown that already at $A = 10^{-5}$ a significant electrostatic gap has developed.

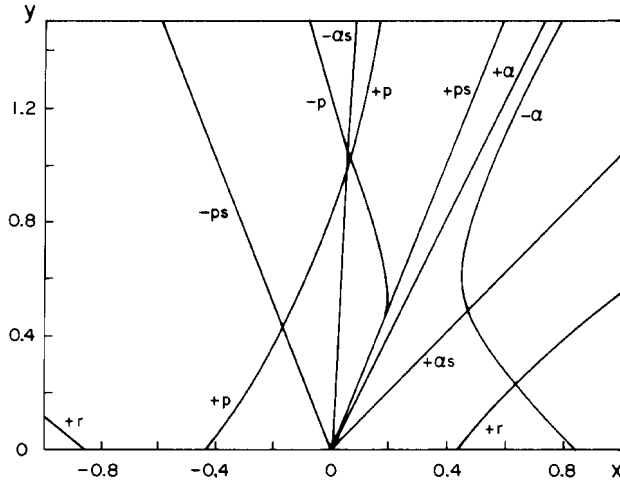


Figure 23. Same as Fig. (20) (α branch) for $\beta_{e,p} = 0.08$ and $\beta_\alpha = 0.8$.

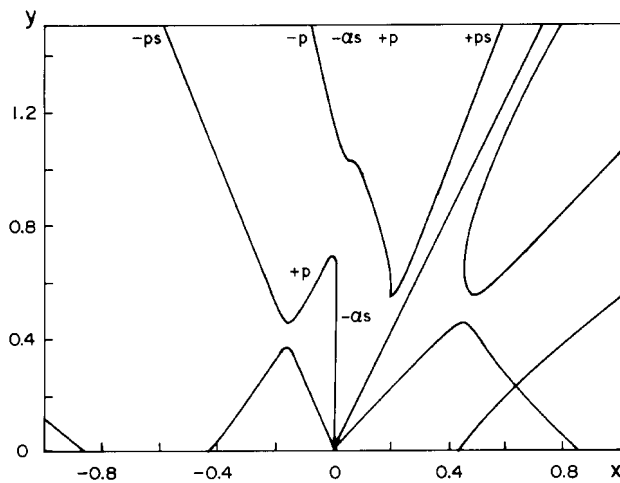


Figure 24. Same as Fig. (23) but for $A = 10^{-4}$. Note the elimination of the electromagnetic decay $(-p, +p)$ (see text).

X. Summary and conclusions

Parametric decays of large amplitude Alfvén waves have been thoroughly investigated over the last 20 years [Galeev and Oraevskii, 1963; Lashmore-Davies, 1976; Goldstein, 1978; Sakai and Sonnerup, 1986; Hoshino and Goldstein, 1989; Viñas and Goldstein, 1991a,b]. However, all these studies have considered only one ion-species. Recently, minor heavy ion species have been considered by Hollweg et al. [1993] and by Gomberoff

et al. [1994a,b,c], showing that heavy ion components cannot be excluded from any realistic treatment of multicomponent plasmas.

Thus, we have studied here parametric instabilities of large amplitude EICW in a magnetospheric-like plasma composed of electrons, a minor component of energetic protons, a background of thermal protons, He^+ and O^+ ions. It is well known that the presence of minor heavy ions introduces new branches in the linear dispersion relation of the EICW, which have resonances at the heavy ion gyrofrequency [Gomberoff and Neira, 1983; Kozyra et al., 1984]. Observations on board several satellites have confirmed the predictions of the linear theory [Young et al., 1981; Roux et al., 1982].

After the appearance of the EICW, the O^+ and He^+ ions are heated up to suprathermal energies of about 100 eV. There seems to be little doubt that the EICW are responsible for this phenomenon. However, it seems that linear theory alone is not able to explain the heating of the bulk of the heavy ions [Gendrin et al., 1984], and nonlinear theory is required. To this end, nonlinear decays of EICW with only a minor He^+ ion-component has been investigated [Gomberoff et al., 1994]. It was conjectured that He^+ ions could be preferentially heated by parametric decays, due to Landau damping and resonance absorption.

Here we have included a minor thermal component of O^+ and He^+ ions. The nonlinear dispersion relation, Eq. (41) is now of order 16 and it reduces to the dispersion relation of Gomberoff et al. [1995a] when η_{O^+} in Eq. (41) is set equal to zero. There are 8 sounds in the system carried mainly by the ion-components, two by each species.

We have analyzed in details the parametric decays of the O^+ branch of the dispersion relation. There are five new instabilities: three decay instabilities involving $(-O, +Os)$, $(-O, +Hes)$, $(-O, +cps)$, and two essentially electromagnetic instabilities, one between $(-O, +O)$, and the other a modulational instability between $(+O, +r)$. All of them can lead to O^+ heating either by Landau damping or resonance absorption.

We then study the influence of the O^+ on the He^+ and proton branch of the dispersion relation. The general picture is similar to the one discussed by Gomberoff et al. [1995a]. In the case of the He^+ branch, a comparison between Fig.(7) of Gomberoff et al. [1995a] and our Fig. (4) shows that there is a new decay instability

which involves $(+Os, -He)$, and instead of the modulational instability, which in the absence of the O^+ involves $(+He, +r)$, there is now a new modulational instability between $(-He, +He)$. On the other hand, the proton branch is very similar to the case when there are no O^+ ions (see Fig. 9 of Gomberoff et al., 1995a) except that now there is an additional decay instability which involves $(+Os, -p)$ (see our Fig. 5).

A numerical analysis of the growth/damping rates of the unstable modes shows that they are comparable, or even larger, for the sounds involving the heavy ions [see Galvão et al., 1994]. Thus, unless kinetic effects suppress the instabilities altogether, we expect the cold heavy ion-species to be substantially heated by non-linear decays of EICW. However, in order to make a definite statement about this point, a full kinetic treatment is required.

From Figs. (3), (4), and (5), it follows that the pump wave is stable to parametric decays involving the hot proton sounds for magnetospheric temperatures. Indeed, they always lead to avoiding crossings, except for a very small gap between $(+hps, +r)$ in Fig. 10b of Gomberoff et al. [1994a]. Therefore, the role of the hot species is to provide the free-energy source of the EICW, namely, the thermal anisotropy, but they do not intervene in the parametric decay of the waves. Consequently, even though there are energetic heavy ion components in the magnetosphere, they can be neglected in the study of the parametric instabilities.

The observed O^+ and He^+ energization seems to be favoured along the direction perpendicular to the external magnetic field. This fact would imply that instabilities involving left hand polarized daughter waves belonging to the O^+ and the He^+ branch of the dispersion relation, should play an important role in the energy transfer from the waves to the O^+ and He^+ ions via resonance absorption.

Next, we have discussed the linear stability of the left hand polarized EICW propagating in a three component plasma composed of electrons, protons and a minor component of drifting alpha particles.

For large values of the proton thermal anisotropies, like those frequently observed in high speed solar wind streams at 0.3 AU [Marsch, 1991], both branches of the dispersion relation can be unstable with large values of the growth rates. The maximum growth rate of the proton branch increases with increasing alpha-proton drift velocity, while the maximum growth rate of the alpha particle branch decreases. The reason lies in the fact

that, as U increases, the proton branch separates from the Doppler shifted alpha particle gyrofrequency, while the alpha branch becomes closer and closer to the alpha particle resonance (compare our Fig. 6 with Figure 1 of Gomberoff and Elgueta, 1991).

Having shown that both branches of the dispersion relation can be excited in high speed solar wind streams, we have studied the non linear decay of the waves. Our study is based on the work of Hollweg et al. [1993], but is aimed at a different goal. First, we have explored the alpha particle branch of the dispersion relation. Second, we have studied the proton branch using frequency values of the pump wave within the range of large growth rates of these waves.

The alpha branch gives rise to a number of decay instabilities. Some of them have been discussed before in different plasma configurations or different branches of the spectrum, but others are new. In particular, there is a modulational instability which involves $-p$ and $+\alpha$ wave which is essentially electromagnetic. It deserves a deeper analysis, but this is beyond the scope of this paper. There is also a new decay instability which involves an $+\alpha s$ and a $-\alpha$ wave. Since this instability involves the alpha sound, it can be a new mechanism for transferring energy to the alpha particles via Landau damping.

In the same branch, but for smaller β -values, there is a new modulational instability between $-\alpha s$ and $+\alpha$. This instability can also be important in the energy transfer to the alpha particles via Landau damping.

We then explored the proton branch by choosing for the pump wave an ω -value close to the maximum growth rate of this branch. There are two electromagnetic instabilities involving the $+p$ and the $-p$ waves. Here, it is interesting to emphasize that we have found that the lines $+ps$ and $-\alpha$, that do not cross for $A = 0$, are forced to coalesce by increasing the pump strength, giving rise to a new decay instability. Thus a strong pump can induce the decay of modes that do not satisfy the resonance conditions when the pump intensity is zero.

Finally, we returned to the alpha branch, but we chose for the pump a lower ω -value. This was done in order to show that the nonlinear instability of this branch is not strongly dependent on the position of the pump. We also use this example to show that the system can be unstable to electrostatic perturbations even in the absence of the pump wave, a situation already discussed by Hollweg et al. (1993) for the proton

branch. In this case the linear instability is suppressed by the action of the pump. This configuration has also been used to discuss a case where there is a crossing between three waves. As a result an electromagnetic instability is lost and replaced by an ordinary decay instability.

A general result which applies to both branches of the dispersion relation of the pump wave is that for high frequencies, like the values we have used here, the pump wave is highly unstable to parametric decays. In fact, very small values of the intensity of the pump are sufficient to trigger parametric decays, a result to be contrasted with Hollweg et al. [1993], where much larger values of A are required. This is even more so in the case of the alpha branch.

The present paper is limited in several respects. We have provided a preliminary identification of the instabilities, leaving out completely the study of the growth rates and the problem of the pump strength threshold. It is well known that usually the pump amplitude must exceed a certain threshold for the development of the parametric instability. The threshold depends on the linear damping processes of the waves, generated by kinetic effects. Thus, in a next stage, a kinetic treatment of the couplings is necessary. The formalism introduced by Kaw (1976) for electromagnetic waves and multi-ion species, seems to be a promising starting point. The matrix elements for the coupling of the interacting wave amplitudes must be analyzed to obtain the growth rates and the physical characteristics of the processes. Eventually this examination may reveal the possibility of explosive phenomena. These studies are needed to obtain the higher level of physical description required to consider the saturation of the linear kinetic instabilities of the pump and the energy fluxes, so that specific applications to solar wind particle heating and acceleration may be envisaged. These studies lie beyond the limits of the present work which, as remarked in the introduction, aims only to give an exploratory overview of the parametric processes of the EICW linearly excited resonant alpha and proton branches.

Acknowledgments

Most of the work presented here is the result of a collaboration with Professors G. Gnani and F. T. Gratton, which has been possible thanks to the support of the Vitae Foundation (Brasil), and the Andes Foun-

dation, grant N° C-12600/9 (Chile). I also want to acknowledge partial support from FONDECYT, grant N° 1940360.

Appendix 1

We show here that the EICW formed in a multi-ion species plasma with drifts is a finite amplitude solution of the cold plasma model. The EICW are represented by $\vec{E} = (E_x, E_y, E_z)$ and $\vec{B} = (B_x, B_y, B_z)$. All quantities are functions of z and t only. There is a constant and uniform magnetic field $\vec{B} = (0, 0, B_0)$. The plasma species are indicated by the index l , including electrons. The density, n_0^l , of each component is a constant. Arbitrary drifts along z are allowed, $\vec{v}_0^l = (0, 0, V_0^l)$, but we assume that the influence of the magnetic field induced by the drift current is negligible. Charge neutrality is assumed, $\sum n_0^l q^l = 0$. The wave is associated with motions of the components described by $\vec{v}^l = (v_x^l, v_y^l, 0)$. We set $\vec{U}^l = \vec{v}_0^l + \vec{v}^l$, and start from the cold plasma equations:

$$(\partial_t + \vec{u}^l \cdot \nabla) \vec{u}^l = \frac{q^l}{m^l} (\vec{E} + \frac{1}{c} \vec{v}^l \times \vec{B}).$$

Using the polarization representation, $E = E_x + iE_y$, $B = B_x + iB_y$, and $v^l = v_x^l + iv_y^l$, we can write (from $c\nabla \times \vec{E} = -\partial_t \vec{B}$)

$$\partial_t B = -ic\partial_z E.$$

The equations of motion give

$$(\partial_t + V_0^l \partial_z + i\Omega^l) v^l = \frac{q^l}{m^l} (E + \frac{V_0^l}{c} B),$$

($\Omega^l = q^l B_0 / m^l c$), and the fact that v^l and B are parallel. From

$$c\vec{\nabla} \times \vec{B} = \partial_t \vec{E} + 4\pi\vec{j},$$

it follows that

$$\partial_t E + \sum_l 4\pi q^l n_0^l v^l = ic\partial_z B.$$

Collecting the previous results we may write

$$(\partial_{tt} - c^2 \partial_{zz})E = \sum_l 4\pi q^l n_0^l \partial_t v^l,$$

$$(\partial_t + v_0^l \partial_z + i\Omega^l) \partial_t v^l = \frac{q^l}{m^l} (\partial_t + V_0^l \partial_z) E,$$

where E , v^l , are finite amplitude quantities, since no linearization procedure is involved. For a solution with space-time dependence as $\exp(ikz - i\omega t)$, putting $\bar{\omega}^l = \omega - kV_0^l$, we get

$$v^l = \frac{\bar{\omega}^l}{\omega} \frac{1}{(\bar{\omega}^l - \Omega^l)} \frac{iq^l}{m^l} E,$$

and

$$[\omega^2 (1 - \sum_l \frac{\omega_{pl}^2}{\omega^2} \frac{\bar{\omega}^l}{(\bar{\omega}^l - \Omega^l)}) - c^2 k^2] E = 0.$$

We obtain, therefore, the dispersion relation of the EICW in a multiple species plasma with arbitrary drifts. This is an extension of Ferraro's finite amplitude waves [Ferraro, 1955; Barnes and Hollweg, 1974].

Appendix 2

The various quantities which appear in the dispersion relation given by Eq. (14) are defined as follows:

$$L_{\pm} = Y_{\pm}^2 - X_{\pm}^2 / \psi_{\pm} - 4\eta X_{\pm}^2 / \psi_{\pm\alpha}$$

$$R_{\pm} = Y_{\pm} (X_0 - \frac{Y X_0^2}{Y_0 X} + \frac{X_{\pm}}{\psi_{\pm}}) / 2\psi_0$$

$$R_{\pm\alpha} = (2\eta Y_{0\alpha} - \frac{Y X_{0\alpha}^2}{Y_0 X_{\alpha}} + \frac{X_{\pm\alpha}}{\psi_{\pm\alpha}}) / \psi_{0\alpha}$$

$$D = \beta'_e \Delta \eta r_{\alpha} X^2 + \beta'_e \Delta_{\alpha} r X_{\alpha}^2 - \Delta \Delta_{\alpha} (X X_{\alpha})^2$$

$$B_+ = -2\beta'_e B_{+\alpha l} \eta r_{\alpha} X X_{\alpha} + B_{+l} X^2 (\beta'_e \eta r_{\alpha} - \Delta_{\alpha} X_{\alpha}^2)$$

$$B_{+\alpha} = -\beta'_e B_{+l} r_{\alpha} X X_{\alpha} / 2 + B_{+\alpha} X_{\alpha}^2 (\beta'_e r - \Delta X^2)$$

$$B_{-cc} = -2\beta'_e B_{-cc\alpha l} \eta r_{\alpha} X X_{\alpha} / 2 + B_{-ccl} X^2 (\beta'_e r_{\alpha} - \Delta_{\alpha} X_{\alpha}^2)$$

$$B_{-cc\alpha} = -\beta'_e B_{-ccl} r_{\alpha} X X_{\alpha} / 2 + B_{-cc\alpha l} X_{\alpha}^2 (\beta'_e r - \Delta X^2)$$

$$B_{+(\alpha)l} = -\frac{A \psi_{(\alpha)} (Y_+ \psi_{+(\alpha)} X_{0(\alpha)}^2 - Y_0 \psi_{0(\alpha)} X_{+(\alpha)})}{Y_0 Y_+ X_{(\alpha)}}$$

$$B_{-cc(\alpha)l} = \frac{A \psi_{+(\alpha)l} (Y_- \psi_{-(\alpha)} X_{0(\alpha)}^2 - Y_0 \psi_{0(\alpha)} X_{-(\alpha)})}{Y_0 Y_- X_{(\alpha)}}$$

where

$$\Delta = A + r(1 - \beta_p Y^2 / X^2)$$

$$\Delta_{\alpha} = A + r_{\alpha} (1 - \frac{\beta_{\alpha} Y^2}{4X_{\alpha}^2})$$

$$A = (B/B_0)^2$$

$$r_{(\alpha)} = \psi_{0(\alpha)} \psi_{+(\alpha)} \psi_{-(\alpha)}$$

$$\psi_0 = 1 - X_0$$

$$\psi_{0\alpha} = 1 - 2X_{0\alpha}$$

$$\psi_{\pm} = 1 - X_{\pm}$$

$$\psi_{\pm\alpha} = 1 - 2X_{\pm\alpha}$$

$$X_{\pm} = X_0 \pm X$$

$$\begin{aligned}
Y_{\pm} &= Y_0 \pm Y \\
X_{\alpha} &= X - YU \\
X_{0\alpha} &= X_0 - Y_0U \\
X_{\pm\alpha} &= X_{\pm} - Y_{\pm}U \\
\beta &= 4\pi n_p \gamma KT / B_0^2 \\
\beta'_e &= \beta_e Y^2 / (1 + 2\eta).
\end{aligned}$$

References

1. Anderson, B.J., R. E. Erlandson and L. J. Zanetti, *J. Geophys. Res.*, **97**, 3075 (1992)a.
2. Anderson, B.J., R. E. Erlandson and J. L. Zanetti, *J. Geophys. Res.*, **97**, 3089, (1992)b.
3. Barnes, A. and J. V. Hollweg, *J. Geophys. Res.*, **79**, 2302, (1974).
4. Berchem, J. R. Gendrin and M. Ashour-Abdalla, *Eos Trans. AGU*, **64**, 815 (1983).
5. Berchem, J. and R. Gendrin, *J. Geophys. Res.*, **90**, 10, 945 (1985).
6. Chappel, R.C., in *High Latitude Space Plasma Physics*, edited by B. Hultquist and T. Hagfors, (Plenum, New York, 1983) p.251.
7. Cohen, R.H. and R. L. Dewar, *J. Geophys. Res.*, **79**, 4174 (1974).
8. Cornwall, J.M. and M. Shultz, in *Solar System Plasma Physics*, edited by L. J. Lanzeroti, C. F. Kennel, and E. H. Parker, (North Holland, Amsterdam, 1979) vol. 3, p. 165.
9. Cuperman, S., L. Gomberoff and A. Sternlieb, *J. Plasma Phys.*, **13**, 259 (1975).
10. Décréau, P.M.E., C. Beghin and M. Parrot, *J. Geophys. Res.*, **87**, 695 (1982).
11. Derby, N.F.J., *Astrophys. J.*, **224**, 1013 (1978).
12. Erlandson, R.L., L. J. Zanetti, T. A. Potemra, L. P. Block and G. Holmgren, *J. Geophys. Res.*, **95**, 5941 (1990).
13. Ferraro, V.C.A., *Proc. R. Soc. London, A* **223**, 310 (1955).
14. Forslund, D.W., J. M. Kindel and E. L. Lindman, *Phys. Rev. Lett.*, **29**, 249 (1972).
15. Fraser, B.N., *Planet. Space Sci.*, **30**, 1229 (1982).
16. Fried, B.D., and S. D. Conte, *The plasma dispersion function*, (Academic, New York, 1961).
17. Galeev, A.A., and V. N. Oraevski, *Sov. Phys. Dokl., Engl. Transl.*, **7**, 988 (1963).
18. Galvão, R.M.O., G. Gnani, L. Gomberoff and F. T. Gratton, *Plasma Phys. Control. Fusion* **36**, 1679 (1994).
19. Gendrin, R. and A. Roux, *J. Geophys. Res.*, **85**, 4577 (1980).
20. Gendrin, R., *Space Sci. Rev.*, **34**, 271 (1983a).
21. Gendrin, R., edited by B. Hultquist and T. Hagfors, (Plenum, New York, 1983) p. 415.
22. Gendrin, R., M. Ashour-Abdalla, Y. Omura and K. Quest, *J. Geophys. Res.*, **89**, 9119 (1984).
23. Goldstein, M.L., *Astrophys. J.*, **219**, 700 (1978).
24. Gomberoff, L. and S. Cuperman, *J. Geophys. Res.*, **87**, 95 (1982).
25. Gomberoff, L. and R. Neira, *J. Geophys. Res.*, **88**, 2170 (1983).
26. Gomberoff, L. and P. Vega, *J. Geophys. Res.*, **92**, 7728 (1987).
27. Gomberoff, L. and R. Elgueta, *J. Geophys. Res.*, **96**, 9801 (1991).
28. Gomberoff, L., *IEEE Transactions on Plasma Science*, **20**, 843 (1992).
29. Gomberoff, L., F. T. Gratton and G. Gnani, *J. Geophys. Res.* **100**, 1871 (1995a).
30. Gomberoff, L., G. Gnani and F. T. Gratton, *J. Geophys. Res.* **100**, 17, 221 (1995b).
31. Gomberoff, L., F. Gratton and G. Gnani, *J. Geophys. Res.*, **99**, 14, 717 (1994).
32. Hasegawa, A., *Phys. Fluids*, **15**, 870 (1972).
33. Hollweg, J.V., R. Esser and V. Jayanti, *J. Geophys. Res.*, **98**, 3491 (1993).
34. Hoshino, M., and M. L. Goldstein, *Phys. Fluids*, **B1**, 1405 (1989).
35. Inhester, B.A., *J. Geophys. Res.*, **95**, 10, 525 (1990).
36. Isenberg, P.A., *J. Geophys. Res.*, **89**, 2133 (1984).
37. Kaw, P.K., in *Advances in Plasma Physics*, (John Wiley, New York, 1976) vol. 6, p. 207.
38. Lashmore-Davies, C.N., *Phys. Fluids*, **19**, 587 (1976).
39. Lee, Y.C. and P. K. Kaw, *Phys. Fluids*, **15**, 911 (1972).
40. Longtin, M. and B. U. O. Sonnerup, *J. Geophys. Res.*, **91**, 6816 (1986).

41. Marsch, E., in *Space - Space and Solar Physics, Physics of the Inner Heliosphere II*, edited by R. Schwenn and E. Marsch, (Springer-Verlag, Berlin, Heidelberg, 1991) vol. 21, p.45.
42. Mauk, B.H., C. E. McIlwain and R. L. McPherson, *Geophys. Res. Lett.*, **8**, 103 (1981).
43. Mauk, B.H., *J. Geophys. Res.*, **87**, 9107 (1982).
44. Mauk, B.H., *Geophys. Res. Lett.*, **8**, 103 (1983).
45. Roux, A. S. Perraut, J. L. Rauch, C. de Villedary, G. Kremser, A. Korth and D. T. Young, *J. Geophys. Res.*, **87**, 8174 (1982).
46. Omura, Y., M. Ashor-Abdalla, R. Gendrin, and K. Quest, *J. Geophys. Res.*, **90**, 8281 (1985).
47. Sagdeev, R. Z., and A. A. Galeev, *Nonlinear Plasma Theor*, (W. A. Benjamin, Readings, Mass., 1969).
48. Sakai J. I, and U. O. Sonnerup, *J. Geophys. Res.*, **88**, 9069 (1983).
49. Tanaka, M., *J. Geophys. Res.*, **90**, 6459 (1985).
50. Umeki, H., and T. Terazawa, *J. Geophys. Res.*, **97**, 3113 (1992).
51. Viñas, A. F., and M. L. Goldstein, *J. Plasma Phys.*, **46**, 107 (1991)a.
52. Viñas, A. F., and M. L. Goldstein, *J. Plasma Phys.*, **46**, 129, (1991)b.
53. Wong, H. K., and M. L. Goldstein, *J. Geophys. Res.*, **91**, 5617 (1986).
54. Young, D. T., S. Perraut, A. Roux, C. de Villedary, R. Gendrin, A. Korth, G. Kremser and D. Jones, *J. Geophys. Res.*, **86**, 6755 (1981).